1976-03

An investigation of optically revelant turbulence parameters in the marine boundary layer.

Hughes, Michele Marie

Monterey, California. Naval Postgraduate School

AN INVESTIGATION OF OPTICALLY REVELANT TURBULENCE PARAMETERS IN THE MARINE BOUNDARY LAYER

Michele Marie Hughes

NAVAL POSTGRADUATE SCHOOL
Monterey, California

THESIS

AN INVESTIGATION OF
OPTICALLY REVELANT TURBULENCE PARAMETERS
IN THE MARINE BOUNDARY LAYER

by

Michele Marie Hughes

March 1976

Thesis Advisor: K. L. Davidson

Approved for public release; distribution unlimited.

SECURITY CLASSIFICATION OF THIS PAGE (When Data Entered)

REPORT DOCUMENTATION PAGE		READ INSTRUCTIONS BEFORE COMPLETING FORM
1. REPORT NUMBER	2. GOVT ACCESSION NO.	3. RECIPIENT'S CATALOG NUMBER
4. TITLE (and Subtitle) An Investigation of Optically Revelant Turbulence Parameters in the Marine Boundary Layer		5. TYPE OF REPORT & PERIOD COVERED Master's Thesis March 1976 6. PERFORMING ORG. REPORT NUMBER
7. AUTHOR(s) Michele Marie Hughes		8. CONTRACT OR GRANT NUMBER(s)
9. PERFORMING ORGANIZATION NAME AND ADDRESS Naval Postgraduate School Monterey, California 93940		10. PROGRAM ELEMENT, PROJECT, TASK AREA & WORK UNIT NUMBERS
11. CONTROLLING OFFICE NAME AND ADDRESS Naval Postgraduate School Monterey, California 93940		12. REPORT DATE March 1976 13. NUMBER OF PAGES 66
14. MONITORING AGENCY NAME & ADDRESS(if different from Controlling Office) Naval Postgraduate School Monterey, California 93940		15. SECURITY CLASS. (of this report) Unclassified 15a. DECLASSIFICATION/DOWNGRADING SCHEDULE

16. DISTRIBUTION STATEMENT (of this Report)

Approved for public release; distribution unlimited.

17. DISTRIBUTION STATEMENT (of the abstract entered in Block 20, if different from Report)

18. SUPPLEMENTARY NOTES

19. KEY WORDS (Continue on reverse side if necessary and identify by block number)

20. ABSTRACT (Continue on reverse side if necessary and identify by block number)

Empirically derived expressions describing the temperature-structure parameter, C_T^2, in terms of the stability parameter z/L or the Richardson number, Ri, over land were used to analyze data of mean humidity, temperature and wind speed and temperature fluctuations obtained by shipboard measurements over open ocean conditions.

In general, there was little correlation between the spectral analyzed C_T^2 values and z/L or Ri. It is recommended that a different

DD FORM 1 JAN 73 1473 EDITION OF 1 NOV 65 IS OBSOLETE
S/N 0102-014-6601 |
(Page 1)

SECURITY CLASSIFICATION OF THIS PAGE (When Data Entered)

approach be used to obtain C_T^2 estimates and that z/L or Ri be modified to account for the anomalous temperature behavior found over a marine environment.

ABSTRACT

Empirically derived expressions describing the temperature-structure parameter, C_T^2, in terms of the stability parameter z/L or the Richardson number, Ri, over land were used to analyze data of mean humidity, temperature and wind speed and temperature fluctuations obtained by shipboard measurements over open ocean conditions.

In general, there was little correlation between the spectral analyzed C_T^2 values and z/L or Ri. It is recommended that a different approach be used to obtain C_T^2 estimates and that z/L or Ri be modified to account for the anomalous temperature behavior found over a marine environment.

TABLE OF CONTENTS

LIST OF TABLES

LIST OF FIGURES

LIST OF SYMBOLS AND ABBREVIATIONS

C_n	Refractive index-structure parameter
C_T	Temperature index-structure parameter
ρ	Density
ε	Rate of dissipation of turbulent kinetic energy
F	Buoyancy force
f	Temporal frequency
g	Acceleration due to gravity
k	Wave number
$(K.E.)_b$	Buoyant kinetic energy
$(K.E.)_n$	Natural kinetic energy of turbulence
κ	von Karman constant, 0.35
ℓ	Local mixing length
L_o	Lower limit of the inertial subrange (micro-scale)
ℓ_o	Upper limit of the inertial subrange (micro-scale)
N	Rate of dissipation of temperature variance
n	Refractive index
P	Ambient pressure
Q	Water vapor density, gm^{-3}
$\bar{q}$	Mean specific humidity, g/kg
q_*	$= -\overline{w'q'}/U_*$
r	Separation distance in defining structure function
Ri	Richardson number

$S_T(k)$	Temperature variance spectral density
T	Ambient temperature
$\bar{T}$	Mean temperature
T_*	Scaling temperature, $(-\overline{w'T'}/U_*)$
T_{*_v}	Scaling virtual temperature, $T_* + 0.61q_*\bar{T}$
$\bar{U}$	Mean horizontal wind speed
U_*	Friction velocity, $(-\overline{U'w'})^{1/2}$
V	Volume of a fluid particle
W	Work done by buoyant action
z	Height
z/L	Stability parameter ratio of height to the Monin-Obukhov length

ACKNOWLEDGEMENTS

I would like to give special recognition and thanks to Dr. Kenneth L. Davidson for his expert guidance, patience and constant encouragement and support during the completion of this thesis. Many thanks also go to Dr. Thomas Houlihan for his technical assistance in describing the instrumentation aboard the R/V ACANIA.

Much appreciation is extended to Mr. Steve Rinard and Mr. Russ Schwanz for their helpful suggestions and careful analysis of the computer programs developed in this thesis.

Special and warm thanks go to my mother, Lorrayne, for helping me record data from the profiles.

I. INTRODUCTION

The advent of more complex and complete numerical models for analyzing and predicting large scale atmospheric motion has also led to better specifications of the boundary layer. The boundary layer is that region in the first kilometer over the sea which is defined principally by turbulent transfer of momentum and heat. Progress has been made in specifications of mean surface wind fields and hydrostatic stability conditions. These are important parameters for predicting changes in the upper part of the ocean or for estimating boundary fluxes in medium range atmospheric prediction models.

The Navy, however, also requires surface layer specifications with regard to their effect on the propagation of optical waves, and the Naval Postgraduate School has been tasked with providing the basis for prediction of the optical properties of the atmosphere for relevant atmospheric window wavelengths. The objective of such a program would be to relate the optical properties and the optically relevant meteorological parameters of the marine boundary layer to the observable bulk atmospheric parameters.

The micrometeorological quantities which define the bulk meteorological quantities are time-averaged values of wind, temperature and relative humidity measured at multiple levels within the constant flux layer. Optically relevant parameters measured are turbulence induced temperature and humidity fluctuations, their frequency spectra, and the aerosol and fog concentrations. The optical properties measured are the modulation transfer function of the atmosphere, the image wander, its frequency

spectrum, the extinction due to absorption and aerosol/fog scattering, and the optical turbulence-structure function, C_n^2, related to scintillation and defined in more detail in section II. It becomes of prime importance in the investigation of optical properties in a marine environment to compute easily C_n^2. Fortunately, a relationship exists between C_n^2 and the temperature-structure function, C_T^2, which is derived from micrometeorological considerations.

A serious handicap in describing the marine environment in the past has been the lack of data and the fact that available expressions, which are empirical in nature, have only been validated over land.

This study is an examination of data collected over a period of two years under open ocean conditions from the R/V ACANIA. The data are computed with expressions derived by Wyngaard et al (1971) and Friehe (1976). These expressions relate C_T^2 to a stability parameter, either the Richardson number or z/L. Both the temperature-structure function and the stability parameters are defined later in this manuscript.

II. THEORETICAL BACKGROUND

A. GENERAL

Turbulence properties of interest in optical propagation are those which could be used to describe the intensity of fluctuations in the refractive index and that which could be used to describe the size or scale of the refractive index inhomogeneities. The former has been related empirically to scintillation, beam spread and beam wander; and the latter along with the former to the image resolution which is important with respect to seeing conditions.

On the basis of the isotropic nature of small scale fluctuation, only one parameter is necessary to describe the intensity of the refractive index fluctuation over many scales. It is the refractive index-structure function parameter, previously mentioned,

$$C_n^2 = \overline{[n(x) - n(x+r)]^2}/r^{2/3} \qquad (1)$$

where $n(x)$ and $n(x+r)$ are refractive indices at two points on a line oriented normal to the mean wind direction and separated by the distance r which is less than the outer scale, L_o, (lower end of the inertial subrange) and greater than the inner scale, ℓ_o (associated with the upper limit of the inertial subrange). The inertial subrange in this spectra is the wave number region where energy is transferred without dissipation from lower to higher wave numbers. See Figure 1.

The refractive index is determined primarily by density fluctuations and can, therefore, be related to temperature fluctuations. C_n^2 is

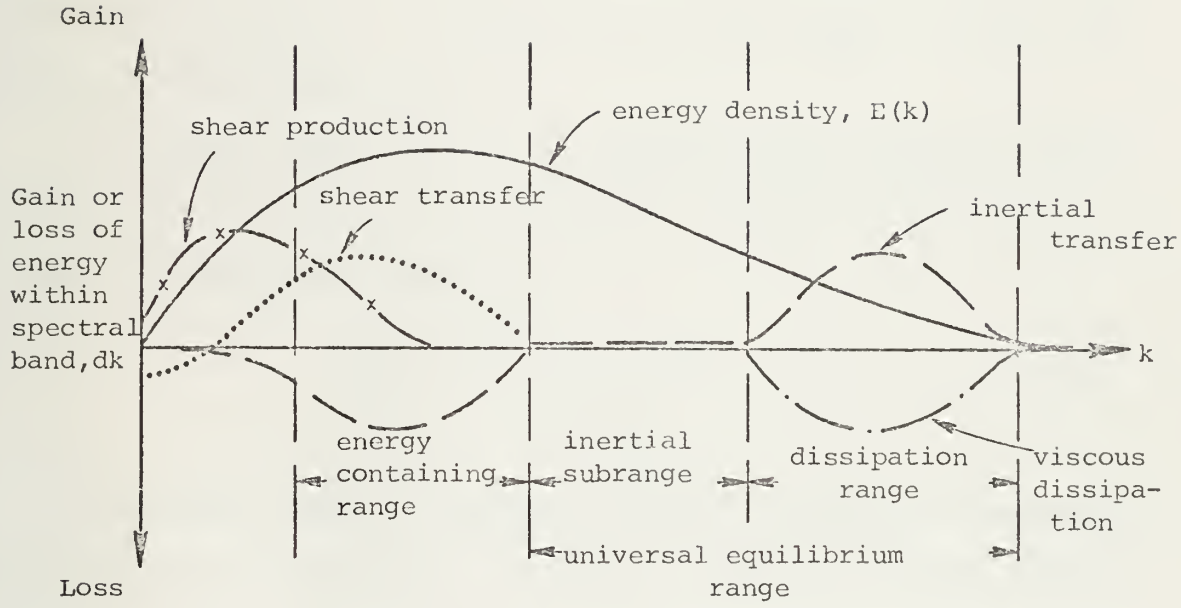

Figure 1. A schematic drawing showing spectral transfer leading to existence of the inertial subrange (Lumley and Panofsky, 1964).

related to the temperature-structure function parameter, C_T^2, by the relation:

$$C_n^2 = \left[\frac{79 \times 10^{-6} P}{T^2}\right]^2 C_T^2 \qquad (2)$$

where C_T^2 can be defined by the temperature variance spectrum, below. This turbulence parameter is the most important variable in determining the optical propagation characteristics of the atmosphere and will be discussed in the next section.

The following expression for the one-dimensional spectral density representation of temperature fluctuation is derived from similarity theory and dimensional analysis:

$$S_T(k) = 0.25\, C_T^2\, k^{-5/3} \qquad (3)$$

As described earlier, turbulence is nearly synonymous with temperature fluctuations; hence it is necessary to describe the mean thermal stratification. Parameters for this are the Richardson number defined by profile measurements or (z/L) defined by flux measurements. These concepts will also be expanded in a later section.

B. CALCULATION OF THE TEMPERATURE-STRUCTURE PARAMETER

There are several methods available to estimate C_T^2 directly and indirectly. These have been partially introduced in previous discussions. The first approach is used to determine C_T^2 directly by the 2/3-law expression for the structure function. In a locally isotropic field, the temperature-structure function has the form

$$C_T^2 = \overline{[T(x) - T(x+r)]^2}/r^{2/3} \qquad (4)$$

at separation r of the order of inertial subrange scales.

A second approach is based on a one-dimensional temperature spectrum, $S_T(k)$, which by definition is the Fourier Transform of the correlation function with separation r in the streamwise direction:

$$C_T^2 = 4\ S_T(k)\ k^{5/3} \tag{5}$$

where k is the streamwise component of wavenumber. Since velocity and temperature fluctuations are measured at a fixed point in the flow, the resultant spectra are realized at a temporal frequency, f. To obtain C_T^2, the temporal (f) and space (k) scales are assumed to be related by Taylor's frozen-field hypothesis, i.e.,

$$k = 2\pi f/\bar{U} \tag{6}$$

where $\bar{U}$ is the mean wind speed at the measurement level. "Frozen" implies that the turbulence pattern remains unchanged as it sweeps past the probe.

The third approach involves measuring separately the rate of dissipation of turbulent kinetic energy (ε) and the rate of dissipation of temperature variance (N) and applying the results to an expression suggested by Corrsin (1951), as another form of the temperature spectrum, viz.,

$$S_T(k) = \beta N \varepsilon^{-1/3}\ k^{-5/3} \tag{7a}$$

which yields the following expression for C_T^2 based on its definition in Equation (5):

$$C_T^2 = \beta N \varepsilon^{-1/3} \tag{7b}$$

(β is an empirical constant evaluated to be 0.25). From this last form, indirect estimates of C_T^2 can be obtained based on mean conditions. This is because ε and N are easily related to boundary fluxes and profiles, if steady and horizontally homogeneous conditions exist. Expressions which relate C_T^2 to mean properties of the boundary layer, such as Ri or z/L, are desirable because the small scale measurements are impractical to obtain in most operational or tactical situations.

Expressions relating C_T^2 to ε and N, Equation (7a), and similarity theory predictions for the dependence of ε and N on momentum and heat fluxes were obtained from examinations by Wyngaard et al (1971):

$$\frac{\varepsilon}{U_*^3 z} = f_1(z/L) \tag{8}$$

$$\frac{N}{T_* U_* z} = f_2(z/L) \tag{9}$$

where $U_* = (-\overline{u'w'})^{1/2}$, $T_* = -\overline{w'T'}/U_*$, $L = -T_o U_*^3/kg\,\overline{w'T'}$ and $f_1(z/L)$ and $f_2(z/L)$ are empirically determined functions.

Direct substitution of Equations (8) and (9) into Equation (7a) yields an expression of the form

$$C_T^2 = T_*^2 z^{-2/3} f_3(z/L) \tag{10}$$

where $f_3(z/L)$ results from the combination of $f_1(z/L)$ and $f_2(z/L)$. Furthermore, since z/L and Ri can be functionally related, a parallel dependence on Ri can be obtained, which is (Wyngaard et al)

$$C_T^2 = z^{4/3} (\partial\bar{T}/\partial Z)^2 f_4(Ri) \tag{11}$$

This final expression provides the desired dependence of C_T^2 on more readily measured parameters (z, $\partial\bar{T}/\partial Z$, and Ri).

C. CONSIDERATION OF THE RICHARDSON NUMBER

1. Derivation of the Richardson Number

McIntosh and Thom (1972) provide a clear and concise explanation of the Richardson number which is the ratio of the buoyant kinetic energy $(K.E.)_b$ to the natural kinetic energy of turbulence $(K.E.)_n$ of a fluid particle in a turbulent boundary layer.

Two reference levels (z_1 and z_2) are chosen within a turbulent boundary layer (shown in typical profiles of velocity, temperature and density in Figure 2), such that, $z_2 = z_1 + \ell$, where ℓ is the local mixing length. In other words, turbulent exchange of each property occurs through the same characteristic distance, or mixing length, ℓ.

The total kinetic energy of a fluid particle of volume V within this boundary layer is made up of two independent components: one associated with the horizontal progress of the particle as part of the mean flow, and the other associated with its own random movements as part of the forced turbulence present in the boundary layer. (The latter is related to the work required to raise the particle from z_1 to z_2 by buoyant action and to the kinetic energy associated with the purely vertical movements of the particle.)

The instantaneous velocity of the particle exceeds the mean value by an amount U' given by $U(z_2) - U(z_1)$; i.e., to a first approximation, $U' = \ell(\partial U/\partial Z)$. McIntosh and Thom also assume that it is justifiable to equate U' and w', so that the vertical component of the 'natural'

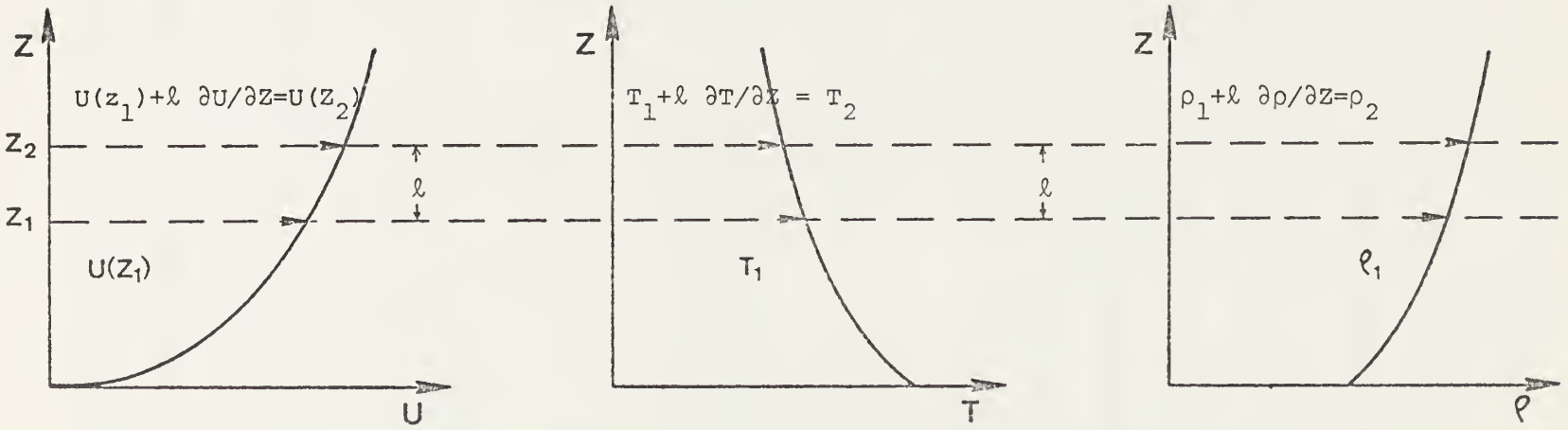

Figure 2. Typical profiles of velocity, temperature and density (McIntosh and Thom, 1969).

kinetic energy of turbulence, $(K.E.)_n$ can be written

$$(K.E.)_n = \frac{1}{2}\rho V w'^2 = \frac{1}{2}\rho V U'^2 = \frac{1}{2}\rho V \ell^2 (\partial U/\partial Z)^2 \qquad (12)$$

Due to turbulent exchange, the fluid particle initially at z_1 and with density ρ_1 appropriate to that level, will find itself at level z_2 and in surroundings of density ρ_2. At level z_2, therefore, the particle is subject to a positive buoyancy force of magnitude $g(\rho_2 - \rho_1)V = F$. Assuming that a linear temperature profile exists locally between z_1 and z_2 and that the buoyancy force acting on the particle increases uniformly from zero at z_1 to F at z_2, the work done (W) by buoyant action is equal to the product of the force $\frac{1}{2}$ F and the distance $(z_2 - z_1)$:

$$W = \frac{1}{2} g(\rho_2 - \rho_1)(z_2 - z_1)V \qquad (13)$$

This amount of work goes directly to increase the upward kinetic energy of the fluid particle, equal to $(K.E.)_n$, by an amount $(K.E.)_b$, to which W may be equated:

$$(K.E.)_b = \frac{1}{2} g(\rho_1 - \rho_2)(z_2 - z_1)V \qquad (14)$$

Finally, on substitution of ℓ for $(z_2 - z_1)$, $\ell \frac{\partial \rho}{\partial Z}$ for $(\rho_2 - \rho_1)$ and $-\frac{\rho}{T}\frac{\partial T}{\partial Z}$ for $\frac{\partial \rho}{\partial Z}$, assuming an incompressible fluid, the equation becomes

$$(K.E.)_b = -\frac{1}{2}\rho V \ell^2 \frac{g}{T}\frac{\partial T}{\partial Z} \qquad (15)$$

The magnitude of the ratio $(K.E.)_b/(K.E.)_n$ indicates the relative importance of free and forced convection in determining the

structure of a fluid boundary layer (shape of velocity profile, nature of turbulence, etc.). The negative of this ratio, or the Richardson number Ri, is a measure of the stability or instability in a region of boundary-layer flow. In lapse conditions Ri is negative, and in inversion conditions, it is positive. After cancelling appropriate terms

$$Ri = \frac{g}{T} \frac{\partial T/\partial Z}{(\partial U/\partial Z)^2} \tag{16}$$

which is one of the forms used in this study.

2. Other Relationships for Richardson Number

The Richardson number Ri can also be expressed in terms of (z/L) or as a bulk aerodynamic formula.

The stability of the surface layer regime determines flux intensities. Monin-Obukhov theory determines the scaling level, L, which is proportional to the level where mechanical and thermal production of turbulent kinetic energy are equal. The ratio of the height of the measurement (z) to the Monin-Obukhov length (L) serves as a stability index (z/L). The Monin-Obukhov length is defined as

$$L = \frac{T_v U_*^2}{q \kappa T_{*_v}} \tag{17}$$

where $T_{*_v} = T_* + 0.61 q_* \bar{T}$, $q_* = -\overline{w'q'}/U_*$, and $\kappa = 0.35$ (von Karman constant).

In unstable conditions the stability parameter z/L is approximately equal to the Richardson number Ri. The following relationships between the stability parameter and Ri have been proposed by Dyer and

Hicks (1970) for an unstable case and Webb (1970) for the stable case:

$$z/L = \frac{Ri}{1 - \alpha\, Ri} \qquad \text{(stable)} \qquad (18)$$

$$z/L = Ri \qquad \text{(unstable)} \qquad (19)$$

Here α is an empirically derived constant equal to 0.5.

A bulk aerodynamic formula is one which relates fluxes across the air/sea boundary to the wind speed at a level and the temperature difference between that level and the surface. The derivation of such a formula involves several assumptions regarding the stability conditions of the boundary layer and the turbulent processes within it. If valid, however, this type of formula is very useful for most practical needs.

Friehe (1976) selected bulk aerodynamic formulae for empirical parameterizations of the surface fluxes of momentum, sensible heat and moisture in terms of average surface layer variables. He used the selected bulk aerodynamic formulae to derive an expression for the estimation of C_T^2 in terms of the relatively easily-measured quantities mean wind, $\bar{U}$, temperature, T, and water vapor density, Q. This formulation by Friehe is presented in the following section.

D. EXISTING EXPRESSIONS AND RESULTS

Wyngaard et al (1971) examined forms of nondimensional expressions relating atmospheric stability to the structure parameter, C_T^2. Dimensional analysis of the height (z), the friction velocity (U_*), the mean potential temperature gradient $(\partial\bar{\theta}/\partial z)$[1], ε, N and C_T^2 produce

---

[1] In this study virtual potential temperature gradients were used to account for humidity gradients over open ocean conditions.

functional expressions dependent only on the Richardson number. Similarity principals are elucidated by using the following Richardson number definition to indirectly obtain a comparable temperature-structure parameter, i.e.,

$$Ri = \frac{g/\bar{T}\ (\partial\bar{\theta}/\partial Z)}{(\partial\bar{U}/\partial Z)^2} \tag{20}$$

This relationship differs from Equation (16) in that the temperature parameter here is a mean potential temperature. When expressed in the finite difference form, a simple approximation to $\partial\bar{U}/\partial Z$, for example, is

$$\left.\frac{\partial\bar{U}}{\partial z}\right|_{z_3} \approx \frac{\Delta\bar{U}}{\Delta z} = \frac{\bar{U}(z_2) - \bar{U}(z_1)}{z_3\ \ell n(z_2/z_1)} \tag{21}$$

where the computed number applies to a geometric mean height defined by $z_3 = (z_1 z_2)^{1/2}$.

Equations including the Richardson number functions (f_1, f_2 and f_4) are equations (8), (9), and (11). Equation (11) relates the temperature-structure parameter and stability parameter and allows for an empirical determination of the f_4 function at varying conditions of stability. If the function f_4 is defined, the temperature-structure parameter can be readily calculated from more easily measured parameters, $\partial\bar{\theta}/\partial Z$ and Ri. In Figure 3 the predicted curve and the data obtained from the extensive 1968 AFCRL study of turbulence structure over a flat, unobstructed Kansas plain are presented. As will be shown in the section describing results, available marine data does not appear to agree with this predicted curve.

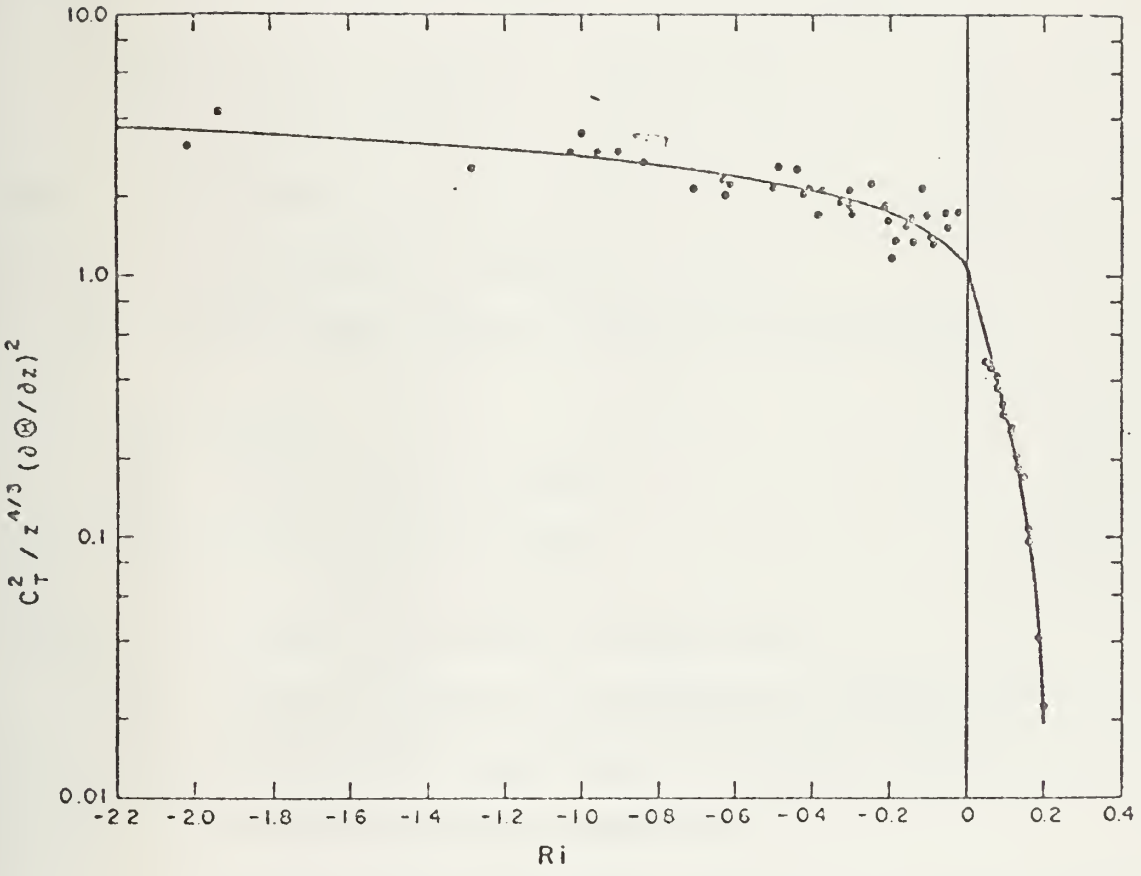

Figure 3. The dimensionless temperature-structure parameter vs. the Richardson number (Wyngaard et al, 1971).

Friehe (1976) combined the semi-empirical equation of Wyngaard et al with the bulk aerodynamic formulae to provide alternate equations for the estimation of C_T^2 in the atmospheric boundary layer above the sea. These equations relate C_T^2 to measurable quantities of average wind speed and air/sea temperature and moisture differences.

The expression derived by Wyngaard et al and considered by Friehe is Equation (10) with f_3 defined as

$$f_3 = 4.9(1 - 7(z/L))^{-2/3} \quad \text{for } z/L \leq 0$$

$$f_3 = 4.9(1 + 2.75(z/L)) \quad \text{for } z/L \geq 0$$

and z = height, m

T_* = characteristic temperature scale, K

The bulk aerodynamic formulae considered by Friehe were

$$U_*^2 = C_D \bar{U}^2 \tag{22}$$

$$\overline{w\theta} = C_H \bar{U}(T_s - T_a) = C_H \bar{U}\Delta T \tag{23}$$

$$\overline{wq} = C_E \bar{U}(Q_s - Q_a) = C_E \bar{U}\Delta Q \tag{24}$$

where $\bar{U}$ = average wind speed at height h, m/s

T_a = average potential air temperature at height h, K

Q_a = average water vapor density at height h, g/m^3

T_s = average sea surface temperature

Q_s = average water vapor density adjacent to the sea surface, usually obtained by assuming the air to be saturated i.e., at dew point T_s, g/m^3

C_D = drag coefficient, from experiment

C_H = sensible heat flux coefficient, from experiment

C_E = moisture flux coefficient, from experiment

h = reference height, usually 10m above the average sea surface

w = vertical velocity fluctuation, m/s

q = moisture fluctuation, g/m^3

θ = potential temperature fluctuation, K

The resulting expressions derived by Friehe and adapted for this study were the following:

For $-20 < \bar{U}\Delta T < 25$ (mK/s):

$$\frac{C_T^2 z^{2/3}}{(\Delta T)^2} = \begin{cases} 3.12 \times 10^{-3} (1 + 1.62X)^{-2/3} & \text{unstable} \\ 3.12 \times 10^{-3} (1 - 0.635X) & \text{stable} \end{cases} \quad (25)$$

where $X = \frac{z\Delta T}{\bar{U}^2} (1 + 0.212 R_3 \Delta Q/\Delta T)$ Ks^2/m

For $\bar{U}\Delta T > 25$ (mK/s):

$$\frac{C_T^2 z^{2/3}}{(\Delta T)^2} = 8.03 \times 10^{-3} (1 + 2.60X')^{-2/3} \quad (26)$$

where $X' = \frac{z T}{\bar{U}^2} (1 + 0.132 R_4 \Delta Q/\Delta T)$

R_3 and R_4 are the ratios of the coefficients used in making adjustments to the levels used for this presentation. Results obtained by Friehe (1976) appear in Figure 4.

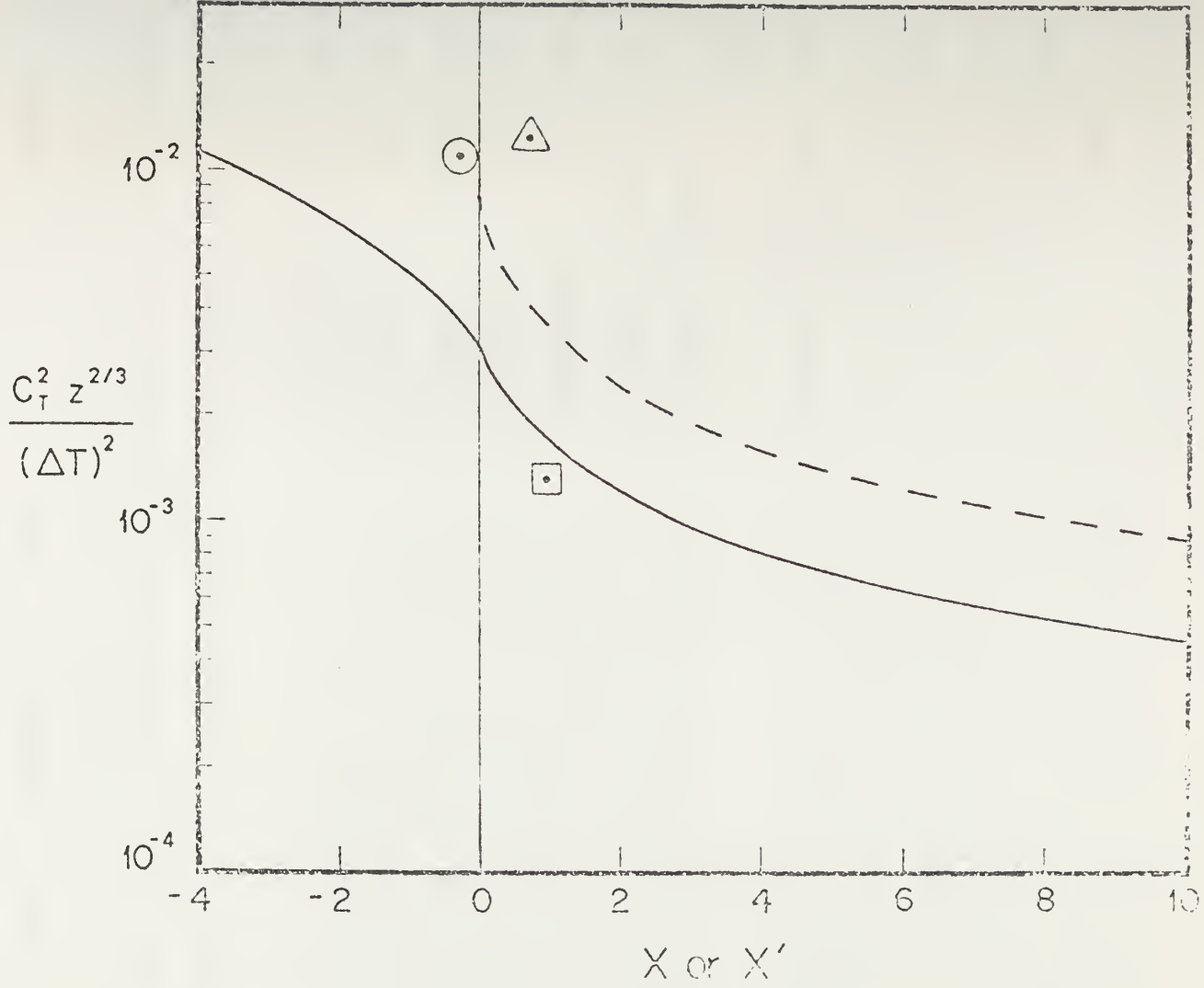

Figure 4. The dimensionless temperature-structure parameter vs. X (Friehe, 1976).

III. THE EXPERIMENT

A. THE PLATFORM AND LOCATION

Observations were obtained aboard the R/V ACANIA anchored off Monterey, California in Monterey Bay. Measurements were made at four levels on two masts spatially separated on the forward deck of the ship. An illustration of the sensor locations of these masts is shown in Figure 5. The vane and probe arrangement appears in Figure 6. The vane maintained a one-dimensional profile of the wind during measurements.

The location of Monterey Bay provided an ideal site for the experimental program as shown in Figure 7. Open ocean differs from land in the effects of wave action on turbulence, in the nature of the aerosols and fog, and to a lesser degree but perhaps significantly on the humidity fluctuations. These conditions can, of course, be best obtained far at sea. The cost of such activities makes it desirable to work near land. Pt. Pinos and Monterey Bay provide very nearly the ideal situation.

Pt. Pinos projects northwest from the mainland toward the prevailing northwest wind. Even under storm wind conditions, the wind comes from the southwest, still bringing sea air toward shore. The ocean depth surrounding Pt. Pinos is shallow enough that the ACANIA can anchor at any range up to about 15 km to the north and northeast.

The effects of land in producing acceleration of the airflow are very small in the Pt. Pinos-Monterey environment. The shoreline southeast from Pt. Pinos is parallel to the prevailing wind. It rises

LEGEND

$\bar{u}$ Cup Anemometer
$\bar{T}$ Quartz Thermometer
$\bar{q}$ Humidiometer
u' Hot Wire
T' Platinum Wire

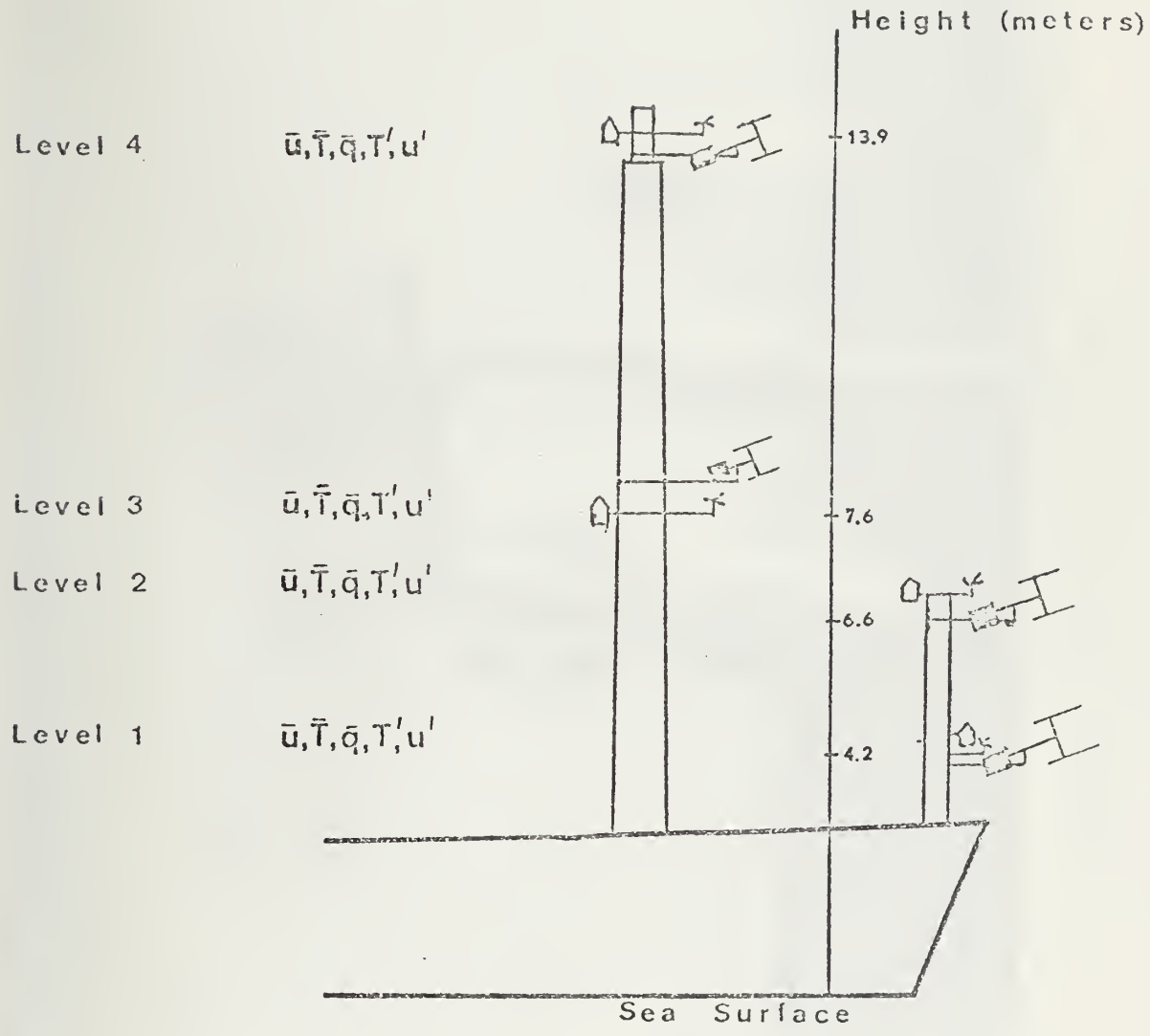

Figure 5. Mounting arrangements aboard the ACANIA.

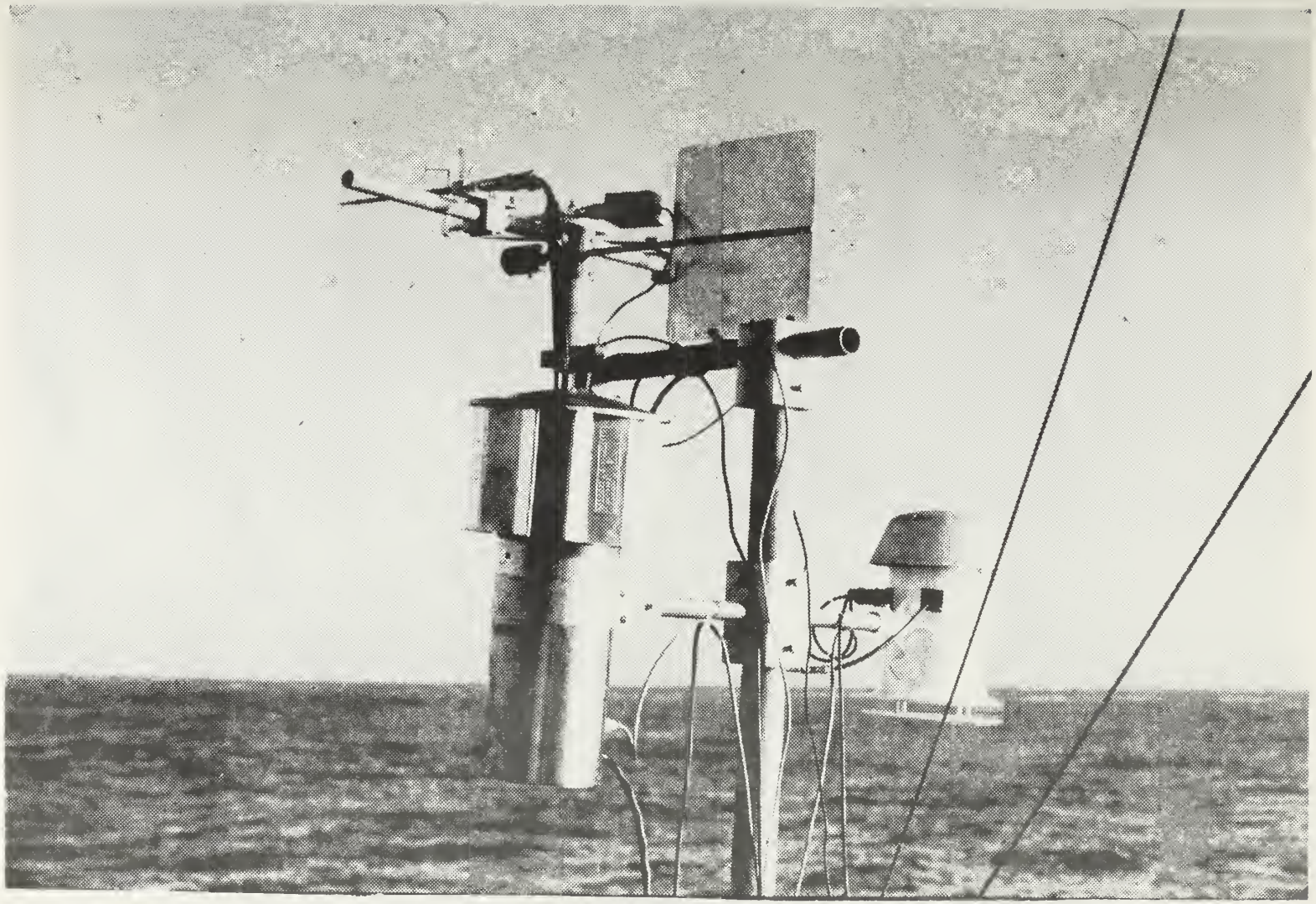

Figure 6. Vane and Probe Arrangement

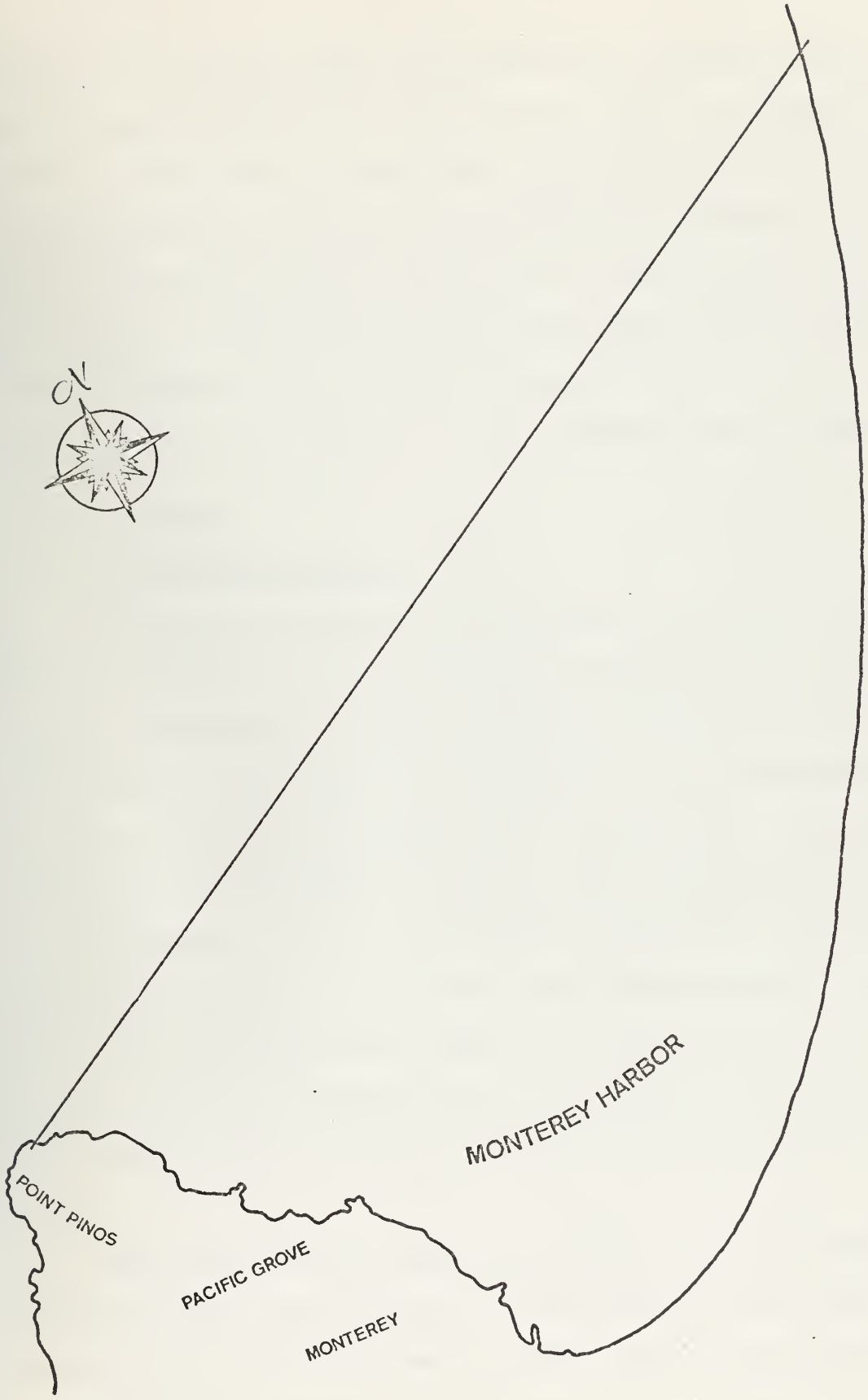

Figure 7. Experimental site in Monterey Bay.

slowly along the water's edge. The eastern edge of Monterey Bay consists of stabilized sand dunes. The sand beach shore is the mouth of the Salinas Valley, about 20 miles wide at the shore line. This valley extends approximately 100 miles to the southeast. In daylight hours, it adds a convective airflow to the southeast. The conventional day-night sea breeze reversal often roughly cancels the prevailing airflow at night to produce a calm period rather than a reversal, so that a relatively small amount of land air is transported out over the water.

B. INSTRUMENTATION

1. Mean Measurement Systems

The mean wind measurements were made with a Thornthwaite Associates cup anemometer wind profile register system, model number 104. In operation the shaft of a three cup anemometer unit serves as the shutter between a light source and a photocell for each revolution. The cups are plastic cones reinforced with aluminum frames. They are attached to the rotating shaft by stainless steel tubing spaced at 120 degree intervals about the shaft as shown in Figure 8. The three cup assembly sets along with the other sensors were positioned at four levels on the bow with electrical leads to the after deck house laboratory. The sets have the characteristics of low starting speeds with a small amount of internal friction which aids in checking inertial overshoot.

Temperature sensitive quartz crystal probes, (Hewlett Packard model HP-2850) were used to measure mean temperatures at each level. RF signals from the crystal probes and from a reference oscillator were mixed in the HP-2801A readout unit to produce a beat frequency whose

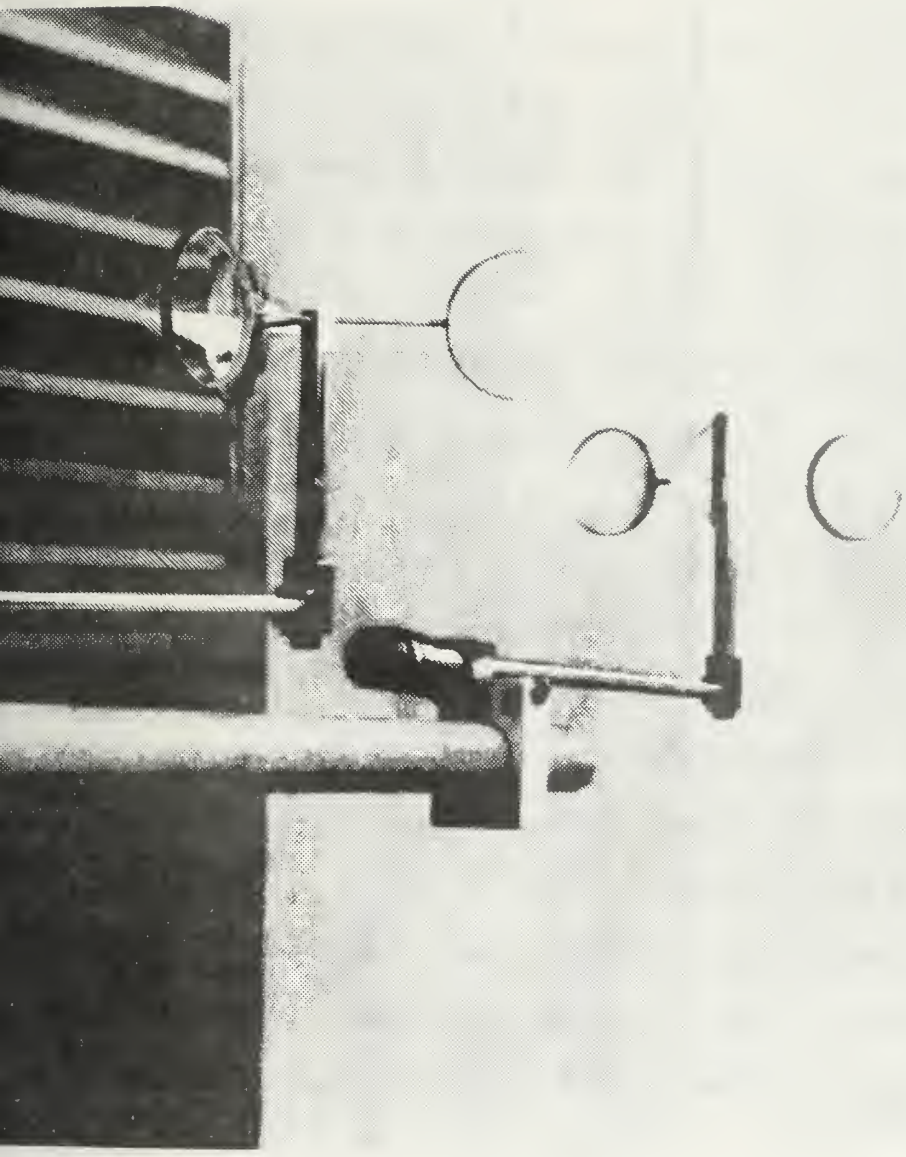

Figure 8. C. W. Thornthwaite Anemometer Cups.

signature can be analyzed to within 0.001 degrees centigrade per hertz. Each sensor simultaneously received pre-experiment calibration against a platinum resistance wire thermometer in a temperature controlled circulating water bath over the expected temperature range. The accuracy in achieving a 0.005 degree centrigrade correction factor was a constant for each probe. A 3.7 meter flexible coaxial cable is permanently attached to the sensor head and the mast mounted probes are housed in an aspirated shelter as depicted in Figure 9. Temperature values were automatically recorded on a printer tape.

The Hygrodynamics Digital I hygrometer indicator and the Dunmore-lithium chloride sensor were used to measure the relative humidity. The Dunmore-type lithium chloride sensor is also pictured in Figure 9. The equipment operates on the basis of resistance change within an electrolytic solution generating a reference voltage variance which is proportional to the relative humidity change. Automatic temperature compensation in the instruments meets the following specifications for relative humidity:

$\pm$ 3% relative humidity below 90%

$\pm$ 4% relative humidity above 90%

Calibration of the sensors was accomplished by comparative methods using saturated salt solutions in an enclosed chamber. Relative humidity was observed and recorded similar to that of temperature as a printed output.

2. Temperature Fluctuation Sensor

The temperature fluctuations were measured using a bridge developed by personnel at GTE Sylvania, the GTE Sylvania Model 140. The system was slightly modified for use in this study.

This system is a small temperature difference sensing device originally designed to be carried aloft by a balloon and equipped to

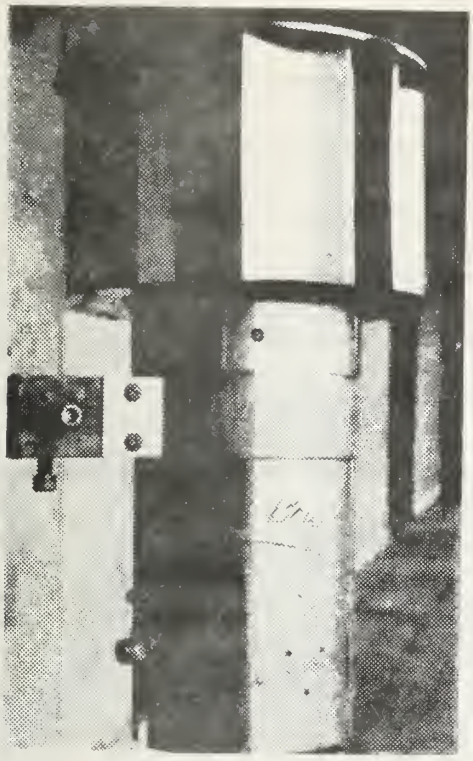

C.C. Breidert Company
Air-X-Houster Type 6L

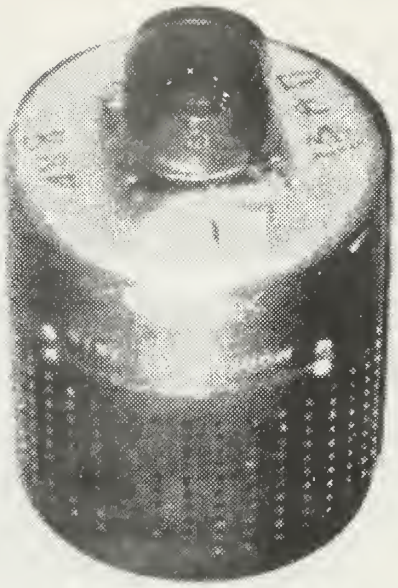

Dunmore-type Lithium
Chloride Sensor

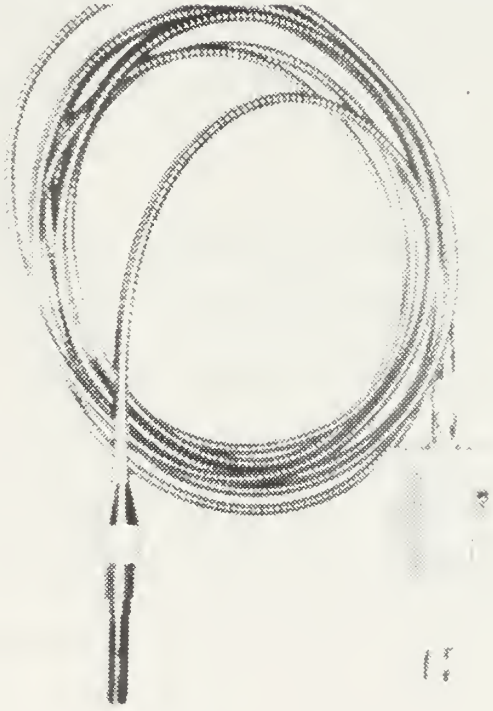

Quartz Thermometer Probe

Figure 9. Photographs of aspirated shelter, hygrometer and thermometer probe.

process and transmit, by pulse-rate modulation on a radio-frequency carrier, this information to a ground-based receiving station for demodulation and recording.

The baseband portion of this system is basically a balanced Wheatstone bridge excited by a 3 kHz signal with a synchronous detector on the output. Segments of a very small diameter platinum wire serve as temperature sensors in opposite arms of the bridge. In the single wire mode, one wire is replaced by fixed resistance. The resistance-temperature coefficients result in an output from the bridge which is proportional to the temperature difference between the two probes or a temperature change of a single wire in the single wire mode.

The sensor wire is 0.5 cm long and 2.5×10^{-6} m in diameter. This extremely small mass allows a response to temperature variations of up to 1 kHz while electronic amplification allows temperature differences as small as 0.004 degrees C to be observed.

C. ANALYSIS PROCEDURES

This particular study was divided into two phases: 1) individual mean wind $\bar{U}$, mean temperature $\bar{T}$, and mean humidity $\bar{q}$ values were plotted on logarithmic scale. Best fit lines were drawn to the points from which data were picked off and applied to the expressions developed by Wyngaard et al; and 2) values of $\bar{U}$, $\bar{T}$, and $\bar{q}$ from individual levels were applied to the bulk aerodynamic expressions examined by Friehe.

Fluctuating temperature T' and profiles of $\bar{U}$, $\bar{T}$ and $\bar{q}$ were studied for eight time periods. Four levels of data were desired, but signals were not always available for all levels due to various component failures. Table I summarizes the periods examined and what data were available for each period.

TABLE I. SUMMARY OF DATA PERIODS

DATE	TIME	NUMBER OF LEVELS	NUMBER OF PROFILES $(\bar{T},\bar{U},\bar{q})$
1974			
27 March	1841-2117	3	12
28 March	1902-2059	3	6
13 August	1700-1742	4	9
18 September	1643	3	3
19 September	1735-2243	3	24
20 September	0014-0552	2,3	15
21 November	1800-2130	4	24
1975			
27 March	1502-2106	2,3	27

Mean wind measurements over ten minute intervals were recorded in a log book. The recordings were the number of cup revolutions for the interval as recorded by electronic counters. Temperature readings were printed on a paper tape from a monitoring digital readout at approximately one second intervals. Relative humidity measurements were recorded the same as the temperatures. All information was later coded and punched on computer cards for further analysis.

The data were then screened for gross errors or inconsistencies due to instrumentation malfunctions. The criterion at this point for retaining or discarding profiles or data periods depended on whether C_T^2 values could be computed from temperature spectra for the time periods involved.

The computer analysis of both phases consisted of programming the governing equations using either actual data or data picked off the profiles. The NPS Fortran program PLOTP was used to plot the predicted curves for phases one and two as well as the results from the data.

1. Profile Editing

The data from $\bar{U}$, $\bar{T}$, and $\bar{q}$ measurements were plotted on 4-cycle semi-logarithmic paper. Since $\bar{U}$, $\bar{T}$, and $\bar{q}$ are parameters which vary logarithmically with height, a best fit straight line was drawn to the data points. In general, the procedures were subjective. In many instances several different slopes could be obtained from just one graph, so a useful criterion was not to give a single data point too much influence in determining the straight line. Consequently, the line drawn represented a most probable position between data points as illustrated in Figure 10.

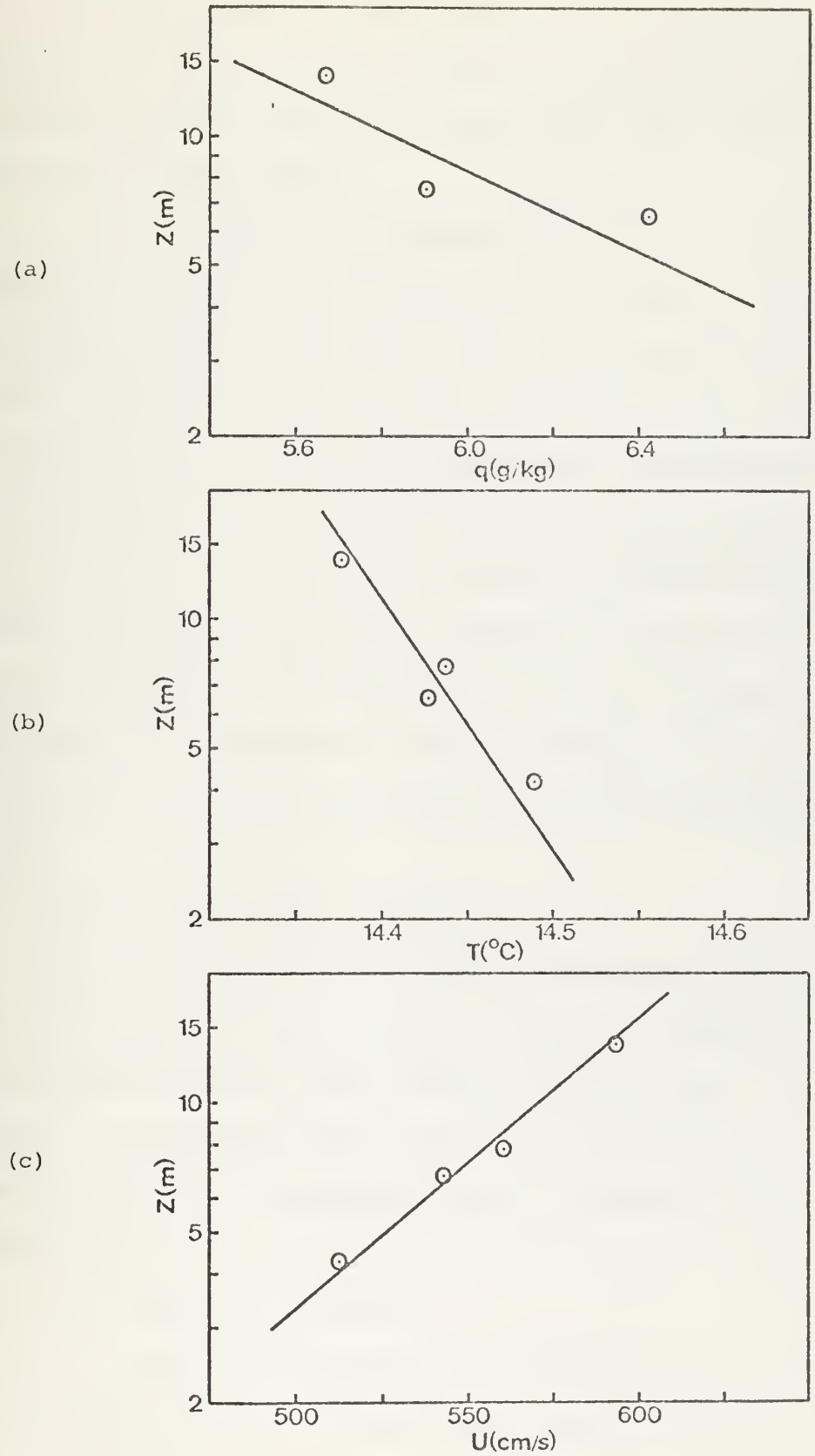

Figure 10. Typical profiles for a) specific humidity - 27 Mar 75 (1539); b) temperature - 19 Sep 75 (1736); and c) winds - 21 Nov 74 (1842).

Difficulty arose whenever anomalous points appeared in a graph as in Figure 11 where the temperature at the third level was obviously inconsistent with the second and fourth levels. In a case such as this, the point was merely ignored.

The time period of 21 November 1974 (1817-2130) was particularly difficult to analyze due to the apparent discrepancy of the temperature and humidity sensors at the fourth level from the readings of the other levels. This discrepancy is evident in Figure 12. These sensors were found in later tests to be out of calibration, and the decision was made to draw the straight line to fit the three lowest levels.

In some, but not in all, cases the sea surface temperature was helpful in determining the slope. However, if the sea surface temperature was significantly different from that expected on the basis of the temperatures in an atmospheric profile, it could not be used since the profile temperatures differed in most cases by only hundredths of a degree.

2. Analysis Procedures to Obtain C_T^2

Variance spectra were interpreted to estimate C_T^2. The spectra were obtained using an analog spectral analyzer. Procedures for converting temperature spectral values, obtained with the analog spectral analyzer, to engineering units and then for obtaining the turbulence parameter C_T^2 from the temperature spectral estimates are described in this section.

a. Spectral Plot Scaling

A necessary procedure was to scale the spectral plots in order to relate RMS input voltages to power spectral densities; (variance per unit frequency).

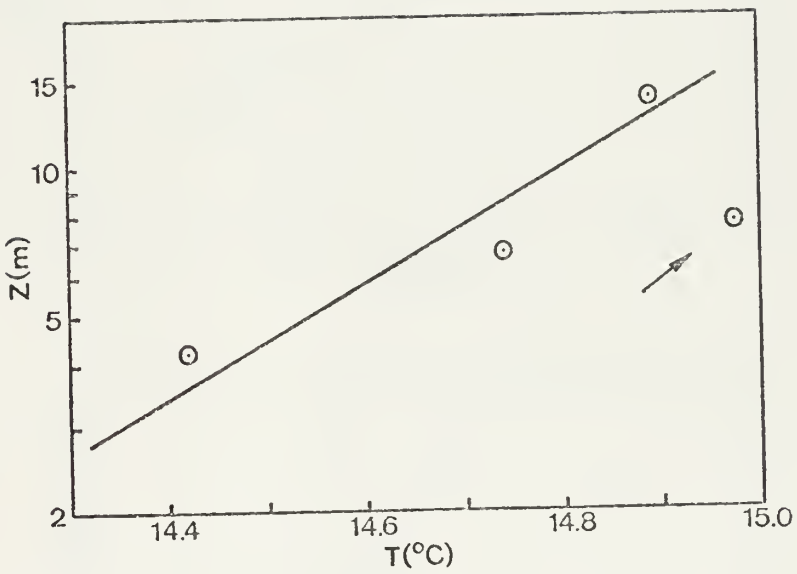

Figure 11. Profile of 27 Mar 74 (1929) showing anomalous temperature reading at third level.

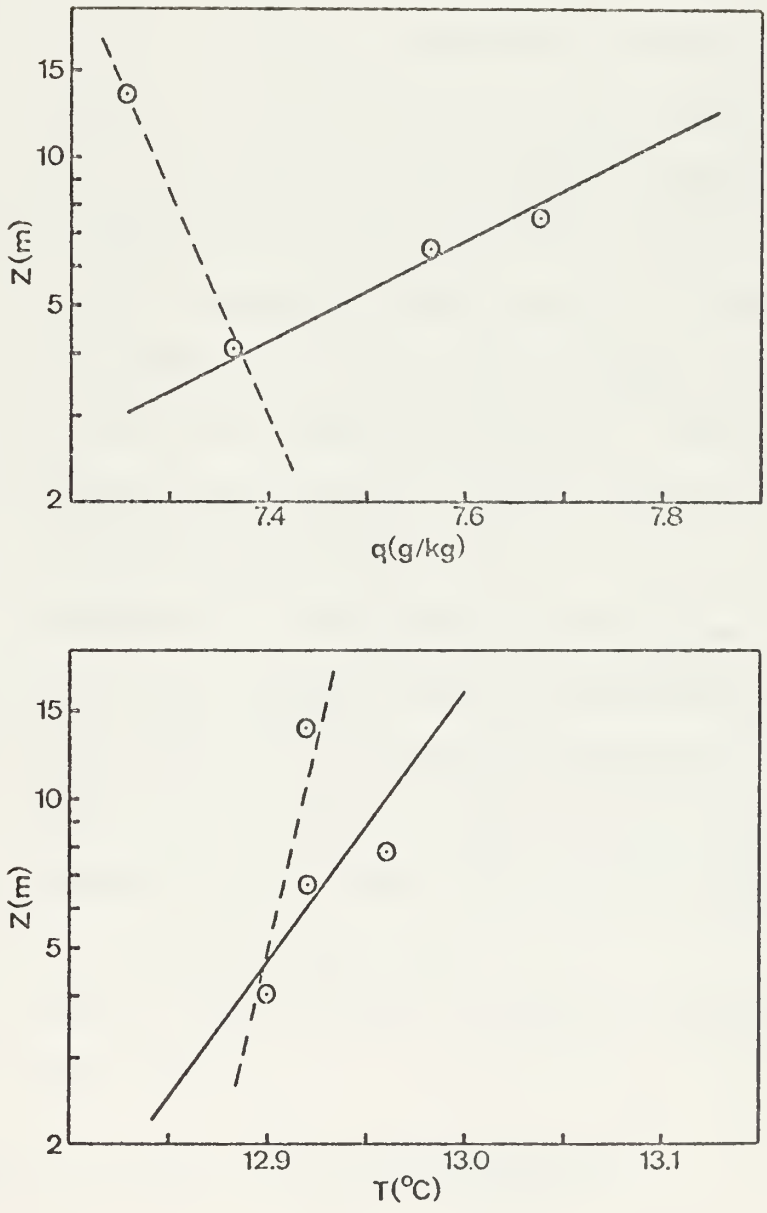

Figure 12. Profiles of 21 Nov 74 (1817). Solid black line represents the profile used.

To obtain power spectral density levels, corresponding to RMS voltage inputs, calibrated scale charts had to be constructed. The charts were constructed as follows. Amplitude scaling was accomplished by using an externally generated signal whose RMS value was determined by a RMS meter. Using a 0-dB (.1v) input gain and a spectral gain of 0-dB (x 1), a signal with amplitude equal to 0.1 volts RMS was produced on a screen display as a spike near the selected frequency. This spike was then plotted with a X-Y plotter. Successively, the input gain was stepped down to attenuate the amplitude of the input signal by 10 dB increments, and plots of the height of each resulting spectral spike or amplitude was then added to the X-Y plot, at different frequencies. These plots represented a graduation of RMS input from a minimum of 0.001 volts RMS to a maximum of 0.1 volts RMS. An example of such a calibration plot on the overlay appears in Figure 13. These procedures were performed regularly during analyses to insure continual calibration of the spectral analyzer and X-Y plotter.

For purposes of the chart format the RMS voltages were converted to LOG 10 units and a graduated scale was constructed so that the logarithm of volts RMS could be interpolated from spectral plots. The amplitude scale was adjusted for each spectrum as a function of both input gain and spectral gain. These values were then converted to PSD levels for use in calculating C_T^2 values.

The equation (based on Federal Scientific specifications) to convert volts RMS to PSD is

$$\text{PSD level } (V^2/Hz) = \frac{0.79 \text{ (cal. level } V_{RMS})^2}{\text{Filter Bandwidth}} \qquad (27)$$

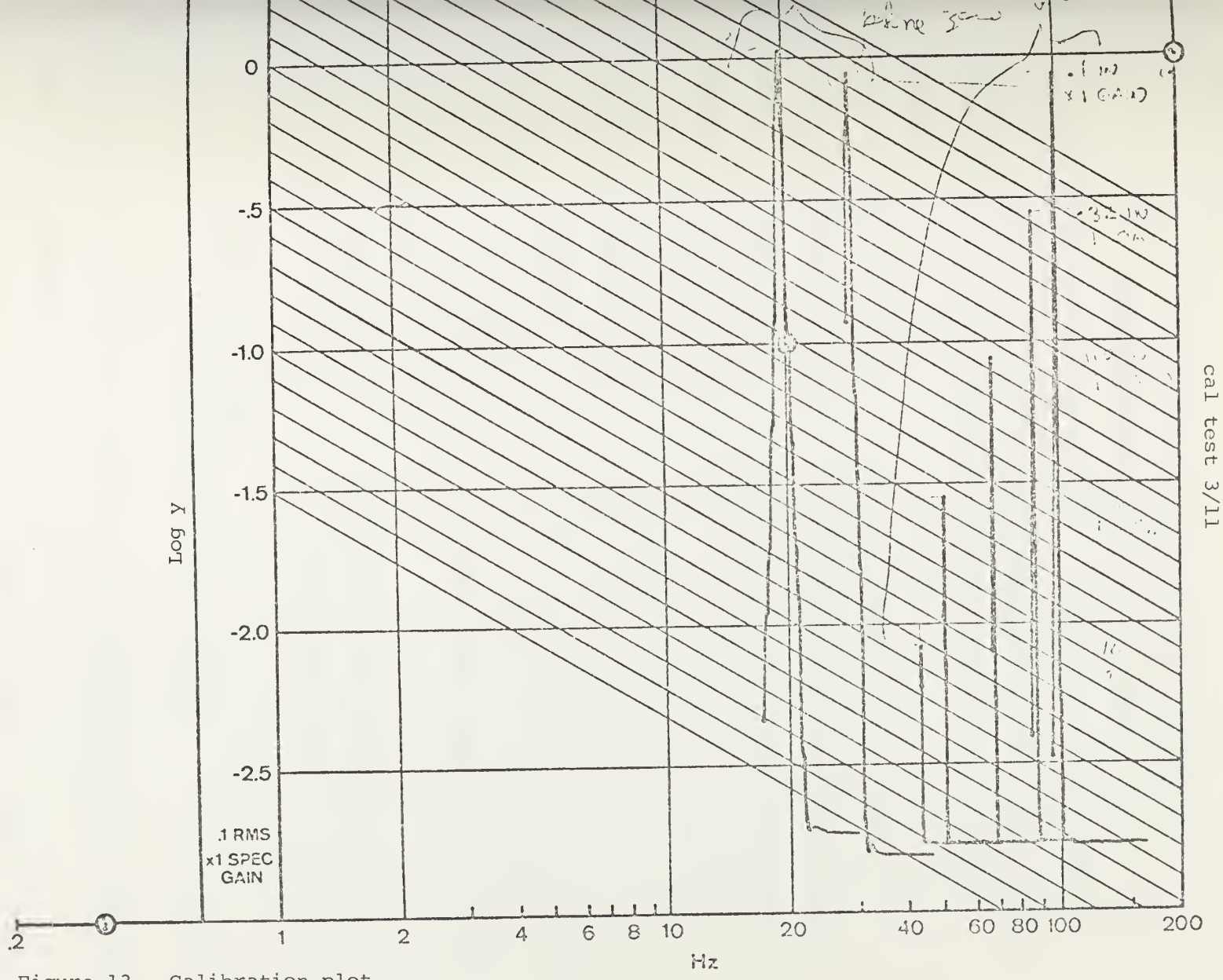

Figure 13. Calibration plot.

where the filter bandwidth ($\beta = 0.4$) is a function of the analysis range selected.

b. Obtaining Turbulence Parameters from Scaled Spectra

The turbulence parameter C_T^2 was obtained from the temperature variance spectra on the basis of the universal formula, Equation (2), for the inertial subrange in wave number space S(k). This expression predicts a -5/3 slope for the spectra when plotted in log-log formats.

Figures 14 and 15 are typical spectra considered in the analyses. Temperature spectra often exhibited slopes slightly different than the expected -5/3. This feature of temperature spectra have been observed by others. The existence of "cold spikes" in temperature traces has been given as a reason for this, e.g., Friehe (1976). A universally accepted reason is still not available, however.

Assuming -5/3 slopes for the variance spectra, S(f), obtained from the analyzer, the intercept of the -5/3 slope with the 1 Hz frequency line was the spectral density denoted (PSD) value used in computing the parameter of interest, C_T^2.

The measured PSD value obtained from temperature spectra was converted to a spectral density in engineering units by the equation

$$S_T(f) = C_H^2 \cdot \text{PSD}$$
$$= (°C/\text{volt})^2 \cdot \text{Volt}^2/\text{Hz} = °C^2/\text{Hz} \qquad (28)$$

where C_H is the calibration factor for the temperature system. Determination of the value for C_H has been described by Lund (1975).

Since the temperature fluctuations were measured at a fixed point in the flow, the resultant spectral values are defined at "temporal" frequencies, f, and are denoted as $S_T(f)$ in equation (28).

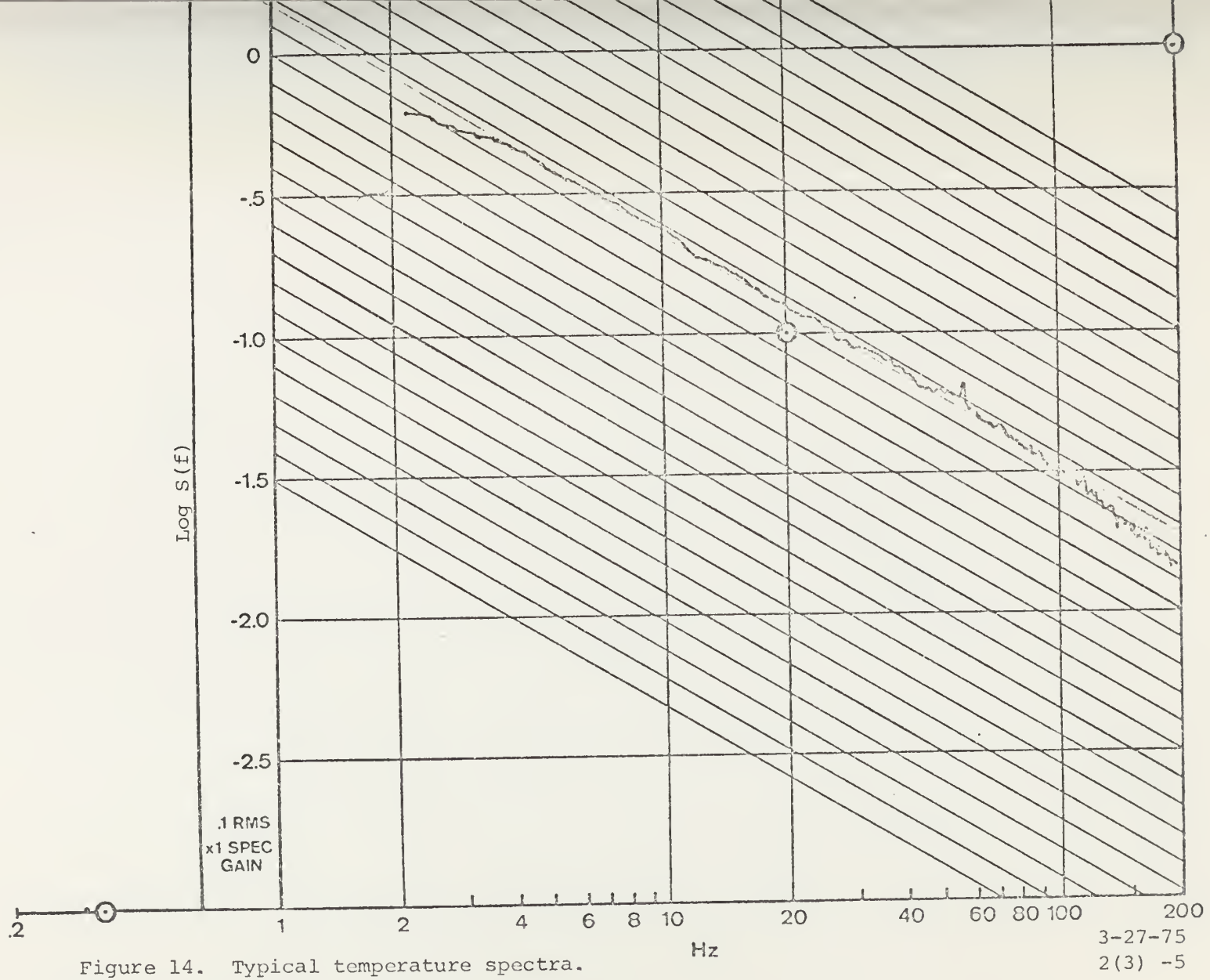

Figure 14. Typical temperature spectra.

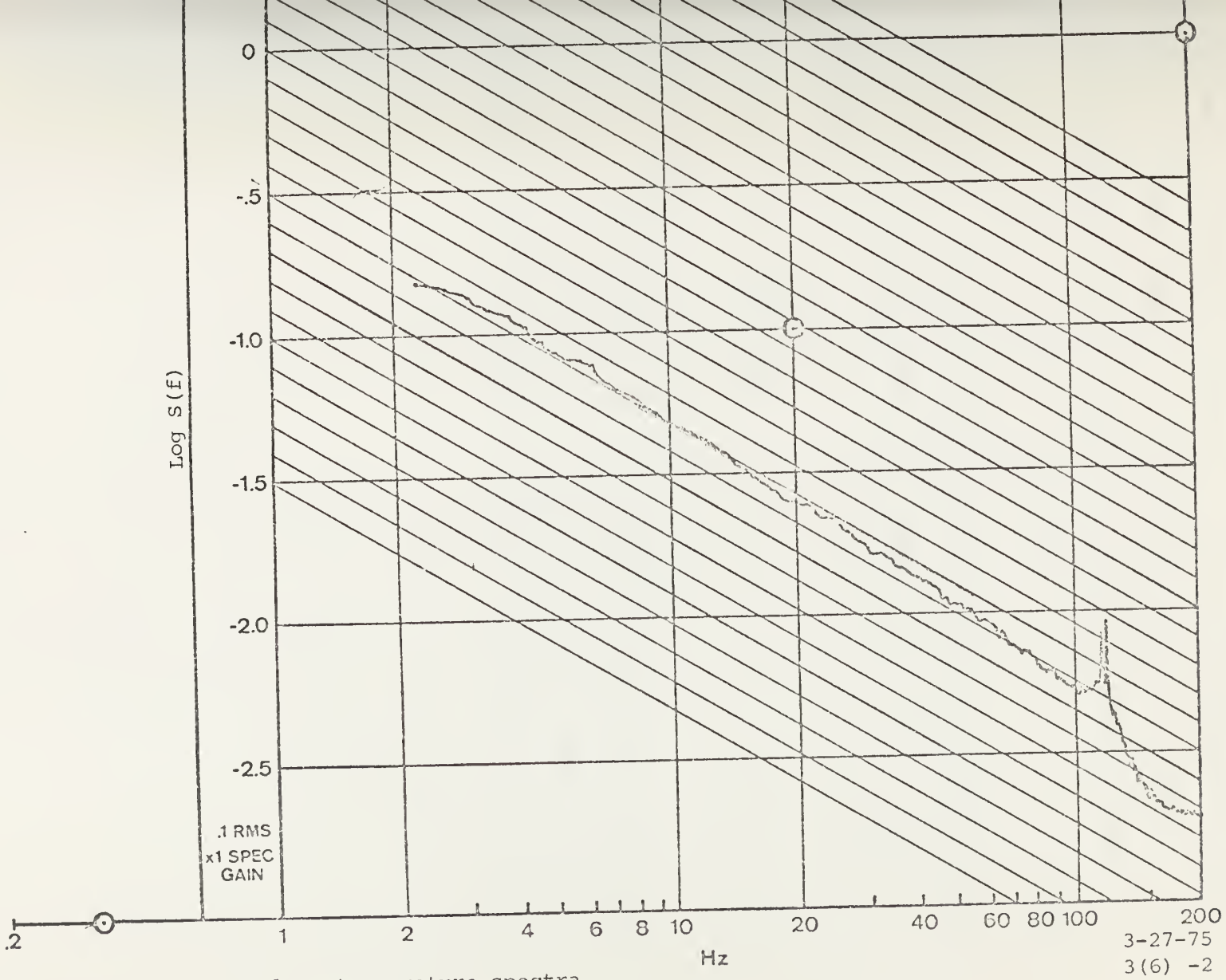

Figure 15. Anomalous temperature spectra.

To obtain C_T^2, temporal (f) and space (k) scales had to be related in order to use Equation (5). This was accomplished by using Taylor's "frozen turbulence" hypothesis discussed in section II,B. The following equation relates temporal to wavenumber spectral values,

$$fS_T(f) = kS_T(k) = c_2 C_T^2 \, k^{-2/3} \tag{29}$$

where $S_T(f)$ is the spectral density value with units of $°C^2/Hz$. This leads to the following relationship between C_T^2 and $S_T(f)$, which is measured,

$$C_T^2 = \frac{k^{2/3}}{c_2} fS_T(f) \tag{30}$$

where, empirically, $c_2 = 0.25$ and $k = 2\pi f/\bar{U}$.

From Equation (30), with measured values of f, $S_T(f)$, and $\bar{U}$, C_T^2 can be determined at each level of interest. These were the procedures used to determine the variation with height of C_T^2 values.

IV. RESULTS

A comparison of the observed results and the Wyngaard et al prediction curve based on Equation (11) appears in Figure 16 where individual data points appear as dots, and averages over Ri intervals of 0.25 appear as dots within a larger circle. The error bars are standard deviations from the mean within each interval, while the number at the top of the error bars is the number of observations defining the mean value.

For both the stable (+ Ri) and unstable (- Ri) stratification cases, there appears to be little agreement and no noticeable trends. The negative Ri numbers were within acceptable ranges from 0.0 to -2.6. The positive values, however, ranged from 0.0 to as high as 35.7. Since turbulence above a critical Ri number is virtually non-existent due to the extreme stability, it was acceptable to assign lower positive Ri values to Ri numbers above 1.0. A critical Ri value is generally considered to be 0.21.

The scatter in the observed results in Figure 16 can be attributed to scatter in both the measured C_T^2 values as well as $\partial\bar{\theta}/\partial Z$ values. Deviation of temperature spectra from -5/3 slope caused uncertainty in C_T^2 estimates. The $\partial\bar{\theta}/\partial Z$ values are important because the temperature gradients are often very small and the quantity is squared for the normalization.

In Figure 17, the results computed by Friehe's bulk aerodynamic expression, Equation (25), are compared to the Wyngaard et al prediction curve. There seems to be some agreement between the observed results

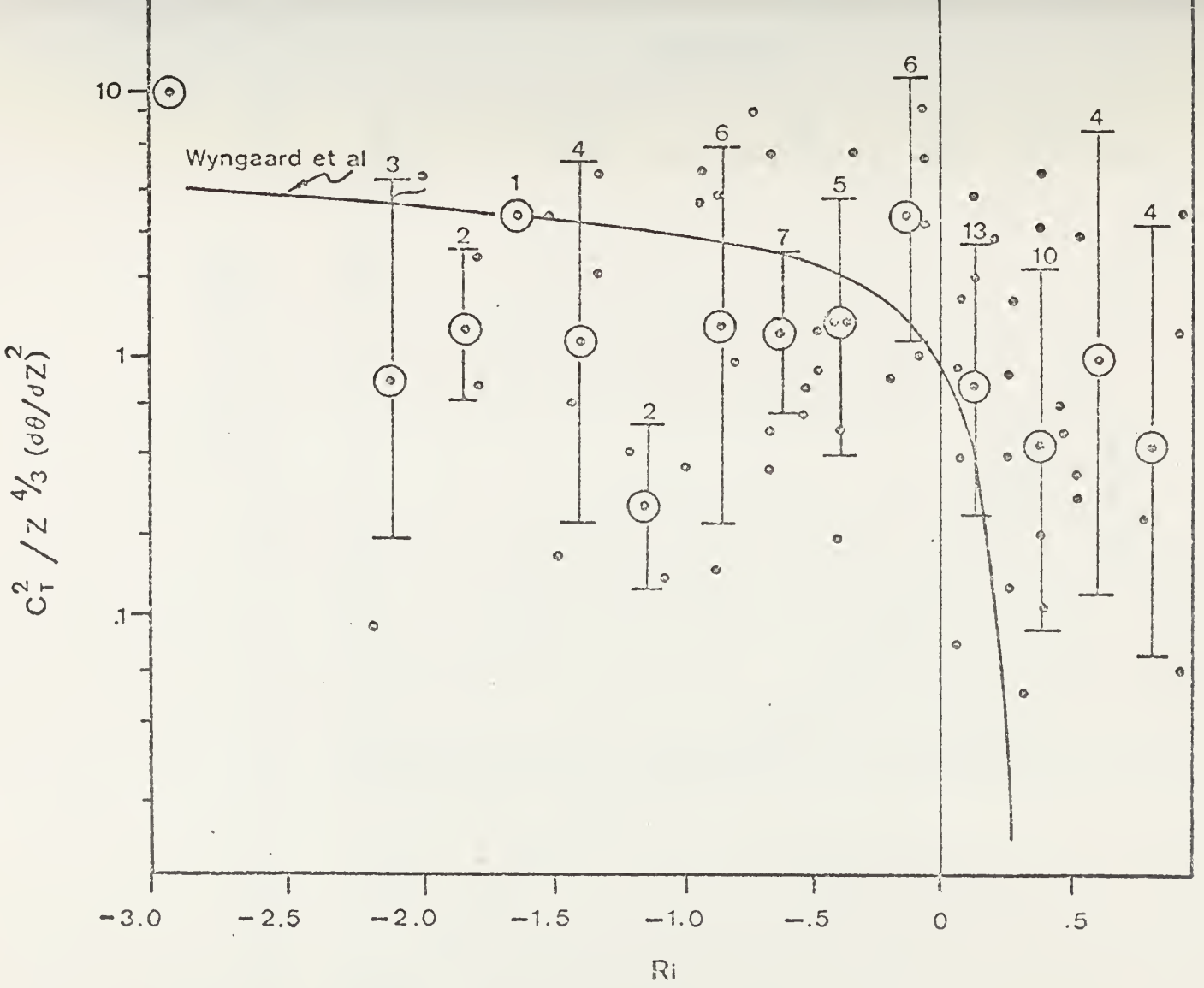

Figure 16. Results of the spectrally derived temperature-structure parameter vs. the Richardson number.

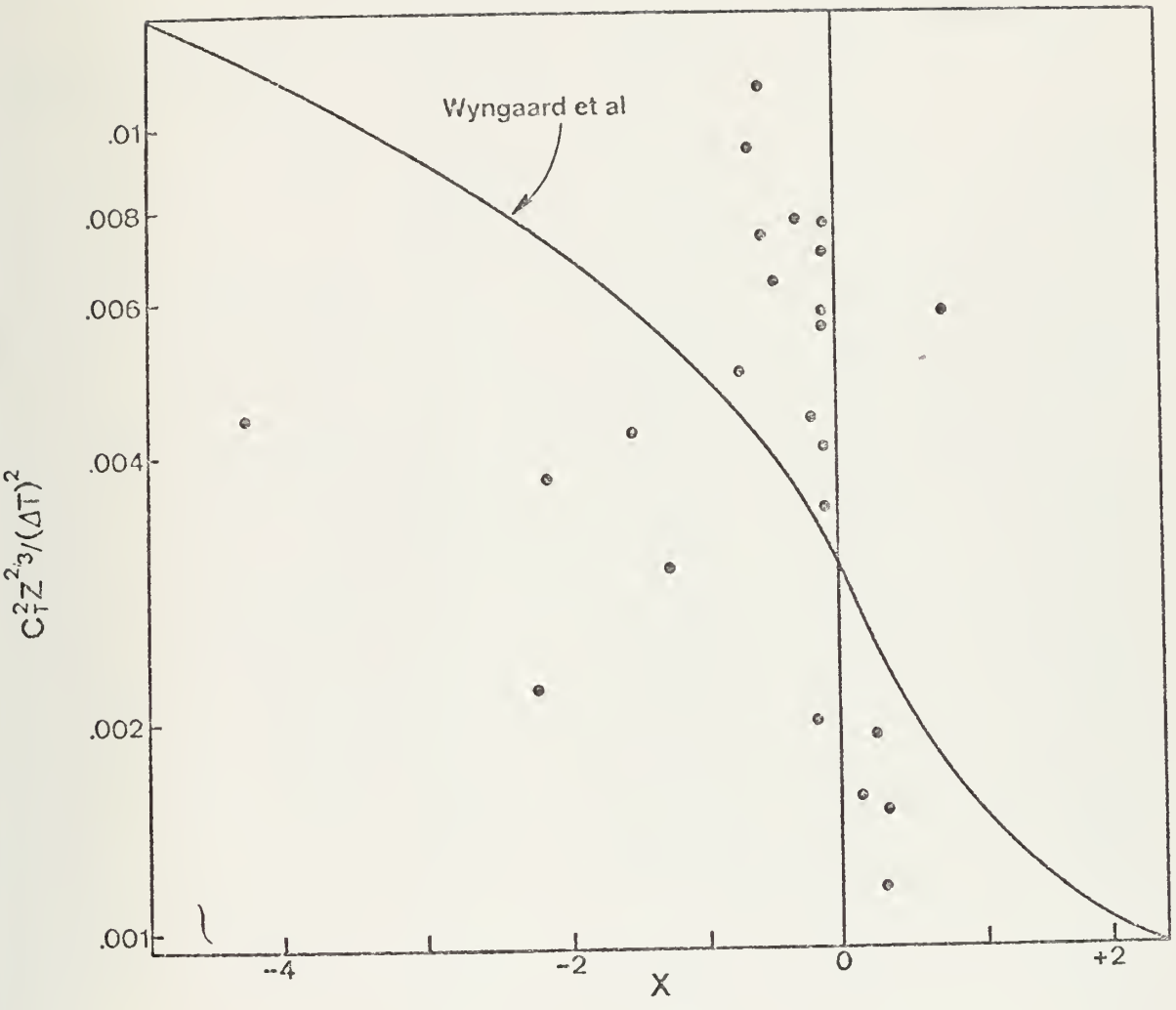

Figure 17. Results of the spectrally derived temperature-structure parameter vs. X.

and the predicted curve close to near-neutral stability conditions, but with the large amount of scatter present, this agreement may be coincidental.

The values obtained for Figure 16 and Figure 17 are summarized in Tables II and III.

TABLE II. C_T^2 and Ri Results

	Period	Level (M)	$d\bar{\theta}/dz$ °C/cm	$C_T^2 \times 10^{-3}$	Ri
1974	3-27-1841	4.19	0.049	1.67	0.362
		6.60	0.031	3.42	0.500
		7.64	0.027	3.37	0.500
		13.89	0.015	-	1.000
	3-27-1902	4.19	0.047	2.07	0.249
		6.60	0.030	2.22	0.392
		7.64	0.026	4.34	0.454
		13.89	0.014	-	0.750
	3-27-1928	4.19	0.047	5.67	0.230
		6.60	0.030	4.98	0.362
		7.64	0.026	6.20	0.419
		13.89	0.014	1.48	0.750
	3-27-2117	4.19	0.019	3.62	0.073
		6.60	0.012	3.22	0.115
		7.64	0.012	-	0.133
		13.89	0.006	1.75	0.242
	3-28-1902	4.19	0.046	17.40	1.000
		6.60	0.029	-	1.500
		7.64	0.025	25.90	1.500
		13.89	0.014	1.80	1.500
	3-28-2059	4.19	0.054	59.60	0.388
		6.60	0.034	-	0.500
		7.64	0.030	30.50	0.500
		13.89	0.016	23.60	1.000
	8-13-1700	4.19	-0.036	4.55	-0.538
		6.60	-0.023	0.895	-0.847
		7.64	-0.020	1.93	-0.981
		13.89	-0.011	0.281	-1.783
	8-13-1721	4.19	-0.036	3.95	-0.665
		6.60	-0.023	0.902	-1.047
		7.64	-0.020	2.44	-1.213
		13.89	-0.011	0.338	-2.204

	Period	Level (M)	$d\bar{\theta}/dz$ °C/cm	$C_T^2 \times 10^{-3}$	Ri
1974	8-13-1742	4.19	-0.025	4.47	-0.451
		6.60	-0.016	0.964	-0.711
		7.64	-0.013	2.30	-0.823
		13.89	-0.007	0.264	-1.496
	9-18-1643	4.19	0.031	0.304	0.308
		6.60	0.020	0.161	0.486
		7.64	0.017	-	0.500
		13.89	0.009	0.140	1.000
	9-19-1735	4.19	-0.005	0.495	-0.082
		6.60	-0.003	2.54	-0.128
		7.64	-0.003	-	-0.149
		13.89	-0.001	0.686	-0.270
	9-19-1846	4.19	-0.005	5.33	-0.100
		6.60	-0.003	22.04	-0.157
		7.64	-0.003	-	-0.181
		13.89	-0.001	1.36	-0.330
	9-19-1900	4.19	-0.010	0.616	-0.607
		6.60	-0.006	1.86	-0.957
		7.64	-0.005	-	-1.107
		13.89	-0.003	1.12	-2.013
	9-19-1929	4.19	-0.005	0.77	-0.099
		6.60	-0.003	2.51	-0.156
		7.64	-0.003	-	-0.180
		13.89	-0.001	1.41	-0.328
	9-19-2011	4.19	-0.010	0.53	0.051
		6.60	-0.006	1.74	0.080
		7.64	-0.005	-	0.093
		13.89	-0.003	0.68	0.169
	9-19-2115	4.19	-0.172	0.37	-3.000
		6.60	-0.109	1.48	-3.000
		7.64	-0.094	-	-3.000
		13.89	-0.052	0.95	-3.000

	Period	Level (M)	$d\bar{\theta}/dz$ °C/cm	C_T^2 x 10^{-3}	Ri
1974	9-19-2158	4.19	-0.010	0.48	-0.202
		6.60	-0.006	2.41	-0.319
		7.64	-0.005	-	-0.369
		13.89	-0.003	1.35	-0.671
	9-19-2243	4.19	-0.178	0.34	-3.000
		6.60	-0.113	1.67	-3.000
		7.64	-0.098	-	-3.000
		13.89	-0.054	1.33	-3.000
	9-20-0014	4.19	-0.011	0.69	-0.461
		6.60	-0.007	4.55	-0.727
		7.64	-0.006	-	-0.841
		13.89	-0.003	1.23	-1.530
	9-20-0056	4.19	-0.013	0.59	-0.408
		6.60	-0.008	-	-0.643
		7.64	-0.007	-	-0.744
		13.89	-0.004	2.32	-1.353
	9-20-0140	4.19	-0.013	0.81	-0.546
		6.60	-0.008	3.06	-0.860
		7.64	-0.007	-	-0.995
		13.89	-0.004	1.10	-1.809
	9-20-0530	4.19	-0.003	0.80	-0.085
		6.60	-0.002	3.79	-0.134
		7.64	-0.002	-	-0.155
		13.89	-0.001	2.05	-0.282
	9-20-0552	4.19	-0.006	0.96	-0.952
		6.60	-0.004	-	-1.500
		7.64	-0.004	-	-1.736
		13.89	-0.002	1.22	-3.000
	11-21-1800	4.19	-1.626	3.93	-3.000
		6.60	-1.032	19.00	-3.000
		7.64	-0.892	7.33	-3.000
		13.89	-0.490	7.18	-3.000

	Period	Level (M)	$d\bar{\theta}/dz$ °C/cm	$C_T^2 \times 10^{-3}$	Ri
1974	11-21-1821	4.19	0.008	3.56	0.027
		6.60	0.005	4.01	0.043
		7.64	0.004	7.14	0.050
		13.89	0.002	2.76	0.091
	11-21-1842	4.19	0.006	3.67	0.033
		6.60	0.004	4.66	0.051
		7.64	0.004	7.66	0.060
		13.89	0.002	11.30	0.108
	11-21-1903	4.19	0.003	5.94	0.009
		6.60	0.002	6.99	0.014
		7.64	0.002	10.90	0.017
		13.89	0.001	1.53	0.030
	11-21-2027	4.19	0.002	8.14	-0.001
		6.60	0.001	3.04	-0.001
		7.64	0.001	13.10	-0.001
		13.89	0.000	1.10	-0.002
	11-21-2048	4.19	0.002	8.81	0.006
		6.60	0.001	10.20	0.010
		7.64	0.001	12.90	0.012
		13.89	0.000	1.68	0.021
	11-21-2109	4.19	-0.000	10.20	-0.025
		6.60	-0.000	15.50	-0.039
		7.64	-0.000	14.90	-0.046
		13.89	-0.000	1.34	-0.083
	11-21-2130	4.19	0.0	11.60	-0.037
		6.60	0.0	17.10	-0.059
		7.64	0.0	21.40	-0.068
		13.89	0.0	2.12	-0.123
1975	3-27-1503	4.19	0.006	11.10	0.004
		6.60	0.004	13.18	0.007
		7.64	0.004	12.45	0.008
		13.89	0.002	-	0.015

	Period	Level (M)	$d\bar{\theta}/dz$ °C/cm	$C_T^2 \times 10^{-3}$	Ri
1975	3-27-1519	4.19	0.006	10.15	0.004
		6.60	0.004	12.66	0.006
		7.64	0.004	5.98	0.007
		13.89	0.002	-	0.012
	3-27-1539	4.19	-0.002	10.55	-0.059
		6.60	-0.001	12.57	-0.092
		7.64	-0.001	9.36	-0.107
		13.89	-0.000	-	-0.195
	3-27-1600	4.19	-0.005	11.25	-0.032
		6.60	-0.003	11.63	-0.051
		7.64	-0.003	9.63	-0.059
		13.89	-0.001	-	-0.107
	3-27-1644	4.19	-0.002	11.82	-0.014
		6.60	-0.001	16.01	-0.023
		7.64	-0.001	10.92	-0.026
		13.89	-0.000	-	-0.048
	3-27-1656	4.19	0.0	11.88	-0.013
		6.60	0.0	12.33	-0.020
		7.64	0.0	7.56	-0.024
		13.89	0.0	-	-0.043
	3-27-2020	4.19	0.041	-	0.016
		6.60	0.026	-	0.025
		7.64	0.022	10.02	0.029
		13.89	0.012	-	0.053
	3-27-2045	4.19	0.044	5.43	0.025
		6.60	0.028	-	0.039
		7.64	0.024	0.72	0.045
		13.89	0.013	-	0.082
	3-27-2106	4.19	0.015	5.73	-0.046
		6.60	0.009	-	-0.072
		7.64	0.008	7.41	-0.083
		13.89	0.004	-	-0.151

TABLE III. C_T^2 and X Results

	Period	Level (M)	$(T_a - T_s)$ °C	$C_T^2 \times 10^{-3}$	X
1974	3-27-1841	4.19	2.76	1.67	-
		6.60	3.06	3.42	0.3121
		7.64	3.18	3.37	0.3688
		13.89	3.22	-	-
	3-27-1902	4.19	2.89	2.07	-
		6.60	3.23	2.22	0.2796
		7.64	3.32	4.34	0.3266
		13.89	3.32	-	-
	3-27-1928	4.19	2.97	5.67	-
		6.60	3.30	4.98	0.1966
		7.64	3.54	6.20	0.2381
		13.89	3.45	1.48	0.4268
	3-27-2117	4.19	3.25	3.62	-
		6.60	3.57	3.22	0.2418
		7.64	3.59	-	-
		13.89	3.63	1.75	0.4863
	3-28-1902	4.19	0.86	17.40	-0.3101
		6.60	0.99	-	-
		7.64	0.98	25.90	0.3046
		13.89	1.32	1.80	0.7809
	3-28-2059	4.19	1.99	59.60	-0.0386
		6.60	2.36	-	-
		7.64	2.37	30.50	0.4924
		13.89	2.60	23.60	1.0340
	8-13-1700	4.19	-0.59	4.55	-0.1676
		6.60	0.69	0.895	0.0849
		7.64	0.49	1.93	0.0375
		13.89	0.38	0.281	0.0013
	8-13-1721	4.19	-0.70	3.95	-0.1893
		6.60	0.64	0.902	0.0691
		7.64	0.43	2.44	0.0223
		13.89	0.39	0.338	0.0051

	Period	Level (M)	$(T_a - T_s)$ °C	$C_T^2 \times 10^{-3}$	X
1974	8-13-1742	4.19	-0.87	4.47	-0.2270
		6.60	0.34	0.964	-0.0054
		7.64	0.18	2.30	-0.0435
		13.89	0.16	0.264	-0.1194
	9-18-1643	4.19	0.24	0.304	0.0229
		6.60	0.19	0.161	-0.0523
		7.64	0.22	-	-
		13.89	0.41	0.140	0.0443
	9-19-1734	4.19	-0.47	0.495	-0.0821
		6.60	-0.53	2.54	-0.1554
		7.64	-0.52	-	-
		13.89	-0.58	0.686	-0.3492
	9-19-1846	4.19	-0.66	5.33	-0.1453
		6.60	-0.73	22.04	-0.2409
		7.64	-0.70	-	-
		13.89	-0.81	1.36	-0.6136
	9-19-1900	4.19	-0.60	0.616	-0.1542
		6.60	-0.65	1.86	-0.2459
		7.64	-0.62	-	-
		13.89	-0.77	1.12	-0.5920
	9-19-1929	4.19	-0.70	0.77	-0.1395
		6.60	-0.74	2.51	-0.2209
		7.64	-0.66	-	-
		13.89	-0.81	1.41	-0.4974
	9-19-2011	4.19	-0.62	0.53	-0.1174
		6.60	-0.67	1.74	-0.1848
		7.64	-0.61	-	-
		13.89	-0.78	0.68	-0.4478
	9-19-2115	4.19	-0.40	0.37	-0.1036
		6.60	-0.42	1.48	-0.1515
		7.64	-0.37	-	-
		13.89	-0.55	0.95	-0.3878

	Period	Level (M)	$(T_a - T_s)$ °C	$C^2 \times T_{10}^{-3}$	X
1974	9-19-2158	4.19	-0.42	0.48	-0.0673
		6.60	-0.45	2.41	-0.0987
		7.64	-0.38	-	-
		13.89	-0.56	1.35	-0.2496
	9-19-2243	4.19	-0.67	0.34	-0.1702
		6.60	-0.88	1.67	-0.2963
		7.64	-0.76	-	-
		13.89	-0.91	1.33	-0.6489
	9-20-0014	4.19	-1.37	0.69	-0.3783
		6.60	-1.48	4.55	-0.5992
		7.64	-1.44	-	-
		13.89	-1.55	1.23	-1.3172
	9-20-0056	4.19	-1.56	0.59	-1.4922
		6.60	-1.68	-	-
		7.64	-1.69	-	-
		13.89	-1.74	2.32	-4.4630
	9-20-0140	4.19	-1.54	0.81	-1.5780
		6.60	-1.67	3.06	-2.1809
		7.64	-1.66	-	-
		13.89	-1.73	1.10	-5.0870
	9-20-0530	4.19	-1.60	0.80	-0.4668
		6.60	-1.63	3.79	-0.7335
		7.64	-1.61	-	-
		13.89	-1.67	2.05	-1.5530
	9-20-0552	4.19	-1.69	0.96	-0.6111
		6.60	-1.72	-	-
		7.64	-1.69	-	-
		13.89	-1.82	1.22	-2.2413
	11-21-1800	4.19	0.54	3.93	0.0107
		6.60	0.57	19.00	0.0393
		7.64	0.63	7.33	0.0552
		13.89	0.58	7.18	0.0480

	Period	Level (M)	$(T_a - T_s)$ °C	$C_T^2 \times 10^{-3}$	X
1974	11-21-1821	4.19	0.51	3.56	0.0136
		6.60	0.53	4.01	0.0373
		7.64	0.57	7.14	0.0591
		13.89	0.53	2.76	0.0452
	11-21-1842	4.19	0.45	3.67	0.0052
		6.60	0.47	4.66	0.0242
		7.64	0.52	7.66	0.0474
		13.89	0.46	11.30	0.0208
	11-21-1903	4.19	0.38	5.94	-0.0046
		6.60	0.39	6.99	0.0044
		7.64	0.45	10.90	0.0260
		13.89	0.38	1.53	-0.0125
	11-21-2027	4.19	0.05	8.14	-0.0729
		6.60	0.04	3.04	-0.0848
		7.64	0.10	13.10	-0.0760
		13.89	0.10	1.10	-0.2260
	11-21-2048	4.19	-0.01	8.81	-0.1442
		6.60	-0.01	10.20	-0.1637
		7.64	0.05	12.90	-0.1591
		13.89	0.0	1.68	-
	11-21-2109	4.19	-0.03	10.20	-0.1697
		6.60	-0.05	15.50	-0.2066
		7.64	0.0	14.90	-
		13.89	-0.08	1.34	-0.5626
	11-21-2130	4.19	-0.01	11.60	-0.1328
		6.60	-0.02	17.10	-0.1572
		7.64	0.04	21.40	-0.1596
		13.89	-0.06	2.12	-0.4471
1975	3-27-1502	4.19	-0.78	11.10	-0.1804
		6.60	-0.70	13.18	-0.1056
		7.64	-0.77	12.45	-0.1394
		13.89	-0.77	-	-

	Period	Level (M)	$(T_a - T_s)$ °C	$C_T^2 \times 10^{-3}$	X
1975	3-27-1519	4.19	-0.18	10.15	-0.1450
		6.60	-0.35	12.66	-0.0736
		7.64	-0.38	5.98	-0.1009
		13.89	-0.34	-	-
	3-27-1539	4.19	-0.74	10.55	-0.1528
		6.60	-0.71	12.57	-0.0924
		7.64	-0.72	9.36	-0.1164
		13.89	-0.75	-	-
	3-27-1600	4.19	-0.73	11.25	-0.1400
		6.60	-0.69	11.63	-0.0836
		7.64	-0.71	9.63	-0.1035
		13.89	-0.76	-	-
	3-27-1644	4.19	-0.74	11.82	-0.1164
		6.60	-0.62	16.01	-0.0615
		7.64	-0.71	10.92	-0.0825
		13.89	-0.74	-	-
	3-27-1656	4.19	-0.32	11.88	-0.0838
		6.60	-0.43	12.33	-0.0438
		7.64	-0.42	7.56	-0.0537
		13.89	-0.46	-	-
	3-27-2020	4.19	0.85	-	-
		6.60	0.72	-	-
		7.64	1.08	10.02	0.0061
		13.89	1.08	-	-
	3-27-2045	4.19	0.15	5.43	-0.3261
		6.60	0.50	-	-
		7.64	0.60	0.72	-0.1205
		13.89	0.63	-	-
	3-27-2106	4.19	0.34	5.73	-0.2351
		6.60	0.44	-	-
		7.64	0.40	7.41	-0.1566
		13.89	-0.24	-	-

V. CONCLUSIONS

Correlation of spectrally derived C_T^2 results with the stability parameter z/L or with the Richardson number values was not good for these data in a marine environment. The temperature gradient in a marine environment is too small and gives rise to very large C_T^2 values which contribute to the observed scatter. As pointed out by Friehe (1976), a complication in the marine boundary layer is the sometimes anomalous behavior of the temperature field where inertial subranges are not always obtained. Salt spray is also a factor to content with in a marine environment and can be the cause of many problems with instruments exposed to it.

For Navy operational purposes, then, existing empirically derived expressions defined by z/L or the Richardson number may require modification before use in describing the atmosphere over an ocean environment for obtaining C_T^2 indirectly. However, for reasons explained in the preceding paragraph, more measurements using a different approach in computing C_T^2 may lead to better correlation between C_T^2 and an easily defined stability parameter. It should also be noted that the correct empirical relationship, when finally derived, may be different over the marine environment than the curve predicted by Wyngaard et al over land.

LIST OF REFERENCES

1. Corrsin, S. (1951): "On the Spectrum of Isotropic Temperature Fluctuations in an Isotropic Turbulence," J. Appl. Phys., 22, 469-473.

2. Dyer, A. J. and Hicks, B. B. (1970): "Flux gradient relationships in the constant flux layer," Quart. J. R. Met. Soc., 96, 715-721.

3. Friehe, C. A. (1976): "Estimation of the Refractive-Index Temperature Structure Parameter in the Atmospheric Boundary Layer over the Ocean," Applied Optics, (in press).

4. Lumley, J. L. and Panofsky, H. A. (1964): The Structure of Atmospheric Turbulence, Interscience Publishers, John Wiley and Sons, London, 239 pp.

5. Lund, A. B. (1975): Spectral Estimates of Marine Turbulence Data, M. S. Thesis, Naval Postgraduate School, Monterey, California, 63 pp.

6. McIntosh, D. H. and Thom, A. S. (1972): Essentials of Meteorology, Wykeham Publications Ltd, London, 239 pp.

7. Taylor, G. I. (1938): "The Spectrum of Turbulence," Proc. Roy. Soc., 164, 476-490.

8. Webb, E. K. (1970): "Profile Relationships: the Log-Linear Range, and Extension to Strong Stability," Quart. J. R. Met. Soc., 96, 67-90.

9. Wyngaard, J. C., Izumi, Y., and Collins, S. A. (1971): "Behavior of the Refractive Index Structure Parameter Near the Ground," J. Opt. Soc. Am., 61, 1646-1650.

INITIAL DISTRIBUTION LIST

		No. Copies
1.	Defense Documentation Center Cameron Station Alexandria, Virginia 22314	2
2.	Library, Code 0212 Naval Postgraduate School Monterey, California 93940	2
3.	Naval Oceanographic Office Library (Code 3330) Washington, D. C. 20373	1
4.	Director, Naval Oceanography and Meteorology Building 200, Washington Navy Yard Washington, D. C. 20374	1
5.	Prof. Kenneth L. Davidson, Code 51Ds Department of Meteorology Naval Postgraduate School Monterey, California 93940	9
6.	Prof. Thomas M. Houlihan, Code 59Hm Department of Mechanical Engineering Naval Postgraduate School Monterey, California 93940	2
7.	Dr. B. Katz, Code 213 Naval Surface Weapons Center White Oak Silver Spring, Maryland 20910	1
8.	Mr. Steve Rinard Department of Meteorology Naval Postgraduate School Monterey, California 93940	1
9.	Prof. Dale F. Leipper, Chairman, Code 58Lr Department of Oceanography Naval Postgraduate School Monterey, California 93940	1
10.	Lieutenant Allan B. Lund Naval Weather Service Facility Fleet Post Office Seattle, Washington 98762	1

11. Captain A. Skolnick 1
PMS 405
Naval Sea Systems Command
Washington, D. C. 20632

12. Lieutenant M. M. Hughes 1
SMC Box 1313
Naval Postgraduate School
Monterey, California 93940

13. Lieutenant Commander H. E. Atkinson III 1
Commander Cruiser-Destroyer Group 1
Fleet Post Office
San Francisco, California 96601

14. Commander Paul E. Lamey 1
Commanding Officer
Thirteenth Naval District
Seattle, Washington 98115